

## Dynamic response of parabolically confined electron systems

Achim Wixforth, M. Kaloudis, C. Rocke, K. Ensslin, M. Sundaram, J. H. English, A. C. Gossard

### Angaben zur Veröffentlichung / Publication details:

Wixforth, Achim, M. Kaloudis, C. Rocke, K. Ensslin, M. Sundaram, J. H. English, and A. C. Gossard. 1994. "Dynamic response of parabolically confined electron systems." *Semiconductor Science and Technology* 9 (3): 215–40.  
<https://doi.org/10.1088/0268-1242/9/3/001>.

# Dynamic response of parabolically confined electron systems

A Wixforth<sup>†</sup>, M Kaloudis<sup>†</sup>, C Rocke<sup>†</sup>, K Ensslin<sup>†</sup>, M Sundaram<sup>‡</sup>,  
J H English<sup>‡</sup> and A C Gossard<sup>‡</sup>

<sup>†</sup> Sektion Physik, Universität München, D-80539 München, Germany

<sup>‡</sup> Materials Department, University of California, Santa Barbara, CA 93106, USA

**Abstract.** The far-infrared response of electron systems confined in a parabolic potential is investigated experimentally. We present recent studies on cyclotron resonance, intersubband resonance and hybrid modes using various experimental techniques and geometries and compare our experimental findings with theoretical results based on a generalization of Kohn's theorem. We also focus on the far-infrared spectrum of so-called imperfect parabolic wells with intentionally induced deviations from ideal parabolicity. Here, new symmetry-forbidden resonances are observed which yield a sensitive test for a theoretical description. At finite wavevector, intrasubband plasmonic excitations are also possible. We study their dispersion and investigate their interaction with the intersubband modes. If subjected to an in-plane magnetic field, the intrasubband plasmon exhibits a strongly anisotropic dispersion which can be directly related to so-called one-dimensional plasmons. Due to the simplicity of the confining potentials, most of our experimental results can be explained in straightforward ways. Many of our results as well as the theoretical descriptions directly apply to recent investigations of lateral nanostructures and thus may also serve for a better understanding of this rapidly developing field.

## 1. Introduction

The interaction between electron systems in semiconductor quantum well structures and optical fields has been studied intensively over the last two decades [1]. These studies include intersubband absorption, cyclotron resonance in high magnetic fields as well as plasmon emission and absorption. The collective excitation spectrum of an electronic system contains valuable information as it is one of its most fundamental properties. For quasi two-dimensional electron systems (Q2DES, quantum films) as realized in space-charge layers in semiconductors, the study of plasmonic (intrasubband) excitations as well as intersubband transitions has proven invaluable in the characterization and understanding of these systems [2]. More recently [3], the collective excitations in quasi one-dimensional (Q1DES, quantum wires) [4, 5] and quasi zero-dimensional electron systems [6] (Q0DES, quantum dots) have also attracted much attention. This is because in the last few years the realization of lateral nanostructures has become possible; this has yielded a rapidly growing field of interest in semiconductor physics. On the other hand tremendous improvements in semiconductor growth techniques like

molecular beam epitaxy (MBE) nowadays offer the possibility to engineer practically every desired kind of band structure for semiconductor structures.

Here we review some of our recent experimental results on the far-infrared response of electron systems confined in parabolic potentials [7–12, and references therein]. The systems investigated are realized in so-called parabolic quantum wells (PQW). Originally they were proposed as an attempt to realize the theoretical construct of *jellium* by creating a wide, highly mobile quasi three-dimensional electron system (Q3DES) [13]. Such a system in the presence of strong magnetic fields is expected to show interesting and exotic properties: depending on the strength of the field, different kinds of broken-symmetry ground states like spin density and charge density waves or crystallization of the electron system in the form of a Wigner crystal have been proposed [14, 15].

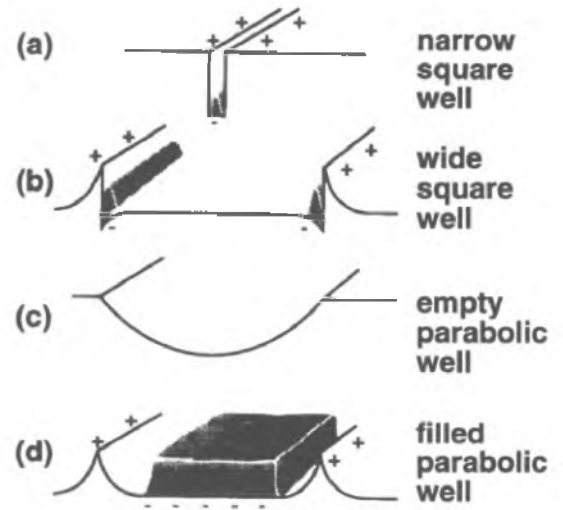
Another very attractive feature of an electron system in a PQW is the striking similarity of many of its properties to those of a Q1DES or even a Q0DES. Many experimental results obtained in such nanostructures have in the recent past been successfully described in terms of a parabolic confining potential [3]. As a matter of fact, early

experiments on the FIR response of a PQW [16, 17] resulted in the generalization of Kohn's theorem [18, 19, 20], which subsequently has been used to explain and understand many interesting properties of laterally confined low-dimensional systems. For these reasons, throughout this review article we shall point out the similarities and the applicability of our experimental and theoretical results to the case of lateral nanostructures and give representative examples.

In section 2 we first give a brief review of some main aspects and features of parabolic quantum wells and the electron systems under investigation. We briefly discuss the fabrication and the characterization of these structures and present some fundamentals of the resulting subband spectrum. Section 3 is devoted to a short description of the generalized Kohn theorem and other existing theories that have been used to model our and others' experimental results. In section 4 we present some experimental details and describe the sample geometries used in our experiments. Section 5 focuses on experimental results and their discussion. We first present some results as obtained in 'ideal' PQW to demonstrate the connection with Kohn's theorem and some other fundamental theoretical models that have been developed in the recent past. We then switch to so-called 'imperfect' PQW, i.e. structures where we intentionally introduce some degree of controlled non-parabolicity to study its influence on the FIR spectrum. We show that we are able to electrically alter specific samples between the 'perfect' and the 'imperfect' state and thus study the influence on, for example, non-local interactions which are also very important in the interpretation of the FIR response of lateral nanostructures. Section 5.3 is devoted to experiments at finite wavevector in the FIR. Here, we use a grating coupler technique to couple to intrasubband plasmonic excitations. Using this technique, we gain access to the complete collective excitation spectrum at small wavevector of an electron slab of finite width, resulting in bulk- and surface-like modes with characteristic dispersion. We study their interaction with the intersubband resonances, and by using an in-plane magnetic field we investigate the field-induced anisotropic band structure of a semiconductor space-charge layer. These experiments are very closely related to the recent observation of one-dimensional plasmons in mesa-etched quantum wires [5].

## 2. Electron systems in parabolic quantum wells

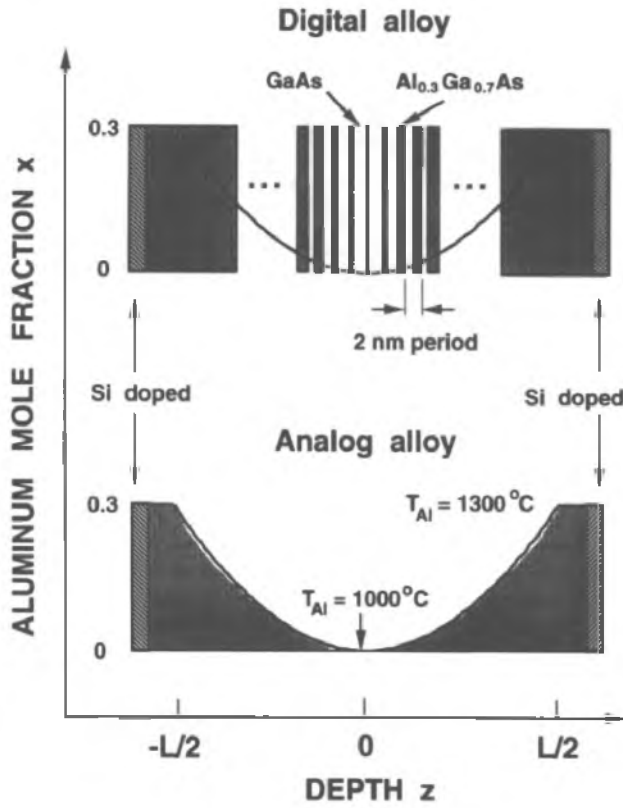
Besides their application in graded-index semiconductor (GRIN-SCH) lasers, parabolic quantum wells were first successfully studied in optical experiments by Miller *et al* [21]. The typical equally spaced energy spectrum of such parabolic structures that has been observed in photoluminescence excitation experiments demonstrated the possibility of a very precise control of molecular beam growth resulting in graded-bandgap structures. The parabolic profiles of both the conduction and the valence bands have been obtained by properly



**Figure 1.** Schematic diagram of different potential energy wells for four different heterostructures, and the corresponding electron distributions. The barriers surrounding the wells are doped in order to supply carriers to the wells. For a narrow square well (a), the electrons are concentrated at the well centre. For a wide square well (b), they repel each other and accumulate at the two interfaces. To obtain an electron gas with uniform density, the well must be graded parabolically (c) to compensate for this electrostatic repulsion. From Poisson's equation, electrons introduced into a parabolic well by doping the barriers (d) distribute themselves uniformly at a density given by the curvature of the parabola. (From [22].)

grading the aluminium content of the ternary  $\text{Al}_x\text{Ga}_{1-x}\text{As}$  alloy. In the range  $0 \leq x \leq 0.3$  the bandgap of  $\text{Al}_x\text{Ga}_{1-x}\text{As}$  varies nearly linearly with the Al mole fraction such that a controlled variation of  $x$  leads directly to the desired structure. Subsequently, remotely doped PQW have been proposed to result in very wide ( $W \leq 0.6 \mu\text{m}$ ) and highly mobile ( $\mu \leq 30 \text{ m}^2 \text{ V}^{-1} \text{ s}^{-1}$ ) quasi three-dimensional electron systems [13]. The basic idea of these structures is to create a conduction band profile  $E_C(z)$  in the growth direction such that it mimics the parabolic potential of a uniformly distributed slab of positive charge.

In figure 1 we depict the basic ideas that led to the realization of such structures [22]. In 1(a), we schematically plot the conduction band profile of a conventional narrow rectangular quantum well in a remotely doped semiconductor heterostructure. Remote doping spatially separates the dopants from the free carriers, thus increasing the electron mobility by a considerable amount. The width of this confining potential is of the order of the de Broglie wavelength of the electrons, and the system forms a Q2DES with quantized levels in the growth direction and a free dispersion along the heterointerfaces. Figure 1(b) depicts the situation for a wide rectangular quantum well. The resulting self-consistent electron distribution is far from being a uniform and wide electron slab. Instead, electrostatics leads to a band bending such that charge accumulates near the edges of the well and in general two independent Q2DES are formed. Such systems, however, are of special interest themselves since here a



**Figure 2.** Realization of a PQW by synthesis of a graded alloy of  $\text{Al}_x\text{Ga}_{1-x}\text{As}$  with parabolically varying Al mole fraction  $x$ . Computer-controlled molecular beam epitaxy is used to create either a digital alloy (top) or an analogue alloy (bottom). The digital alloy is a superlattice consisting of GaAs and  $\text{Al}_{0.3}\text{Ga}_{0.7}\text{As}$  with a 2 nm period as explained in the text. (From [22].)

possibility is given to investigate the properties of coupled electron systems in great detail [23]. Figure 1(c) shows a sketch of the conduction band profile of a graded PQW. Once this structure is remotely doped, the donors release electrons into the well which in turn will screen the man-made parabolic potential, thus forming the wide and nearly homogeneous electron layer shown in figure 1(d). An undoped layer between the dopants and the well reduces ionized impurity scattering and thus enhances the electron mobility in the well as for conventional heterostructures. The bare man-made parabolic potential is equivalent to the potential of a positive charge density  $n^+$ . This fictitious charge is related to the curvature of the grown parabola by Poisson's equation, namely

$$n^+ = \frac{\epsilon\epsilon_0}{e^2} \frac{\partial^2 E_c}{\partial z^2} = \frac{8\epsilon\epsilon_0\Delta}{e^2 W^2}. \quad (1)$$

Here  $\epsilon$  denotes the mean dielectric constant of  $\text{Al}_x\text{Ga}_{1-x}\text{As}$ ,  $\Delta$  is the energy height of the parabola from its bottom to the edges,  $e$  is the electronic charge and  $W$  the width of the grown PQW.


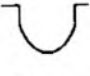


The curvature of the parabola and thus the fictitious charge  $n^+$  can be varied over a wide range by proper control of the growth process. Due to the similarity to a real existing positive space charge this concept has been referred to as 'quasi-doping' in the past [13]. In figure 2, we show the two basic methods that have been

employed to grow PQW by means of MBE. The goal is a graded aluminium profile that can be controlled very precisely. In figure 2(a) we show the technique of the so-called digital alloy. A short-period (2 nm) superlattice of GaAs and  $\text{Al}_{0.3}\text{Ga}_{0.7}\text{As}$  is grown such that the duty cycle between the two species varies quadratically during the growth. The average Al content is then given by the full curve. A prerequisite for this procedure is a very short period of the superlattice with thin wells and barriers to allow for nearly perfect tunnelling between the wells. In figure 2(b) a different, more straightforward technique is shown. By varying the crucible temperature of the aluminium furnace from, for example  $T = 1000^\circ\text{C}$  to  $T = 1300^\circ\text{C}$  one can control the Al flux towards the substrate in a quite controlled manner. The problem, however, is the large thermal inertia of the crucibles which makes it difficult to avoid feedback oscillations of the growth rate. All the samples presented in this report are grown using the digital technique, no important differences having been observed due to the superlattice structure as compared with 'analogue' samples. The actual profile of the Al mole fraction is not easily measured directly. Its general shape is sometimes deduced from optical and electrical measurements on the resulting structures, followed by a fitting of the data to the calculations for the desired energy bandgap profile. However, it is very useful, at any rate, to be able to calibrate the deposited Al mole fraction versus depth in a direct way. The usual way is to employ analytical methods like secondary-ion mass spectroscopy (SIMS) which is, however, quite time-consuming and not straightforward. Recently, we presented a technique [24] which is simple and reproducible, and has reasonable resolution and accuracy. This technique is based on a calibration run directly before growth of the actual PQW and monitoring the Al flux directly using a fast ion gauge scheme. Using this method we were able to calibrate our grown PQW to within  $\Delta x_{\text{Al}} \leq 0.01$  and to show that our digital alloy approach produces more accurate parabolic profiles than we have been able to produce by analogue alloying.

The parameters of the four different samples investigated in this report are listed in table 1 where they are identified by the wafer number. Two different types of parabolic quantum wells are used: (i) three PQW with different curvatures and additional vertical sidewalls (PB25, PB26 and PB31), and (ii) for comparison one PQW (PB48) without vertical sidewalls but with the same curvature as PB25. The difference between PB26 and PB31 is the higher electron mobility of the latter, leading to narrower linewidths in the FIR spectra. Using a conduction band offset between  $\text{Al}_{0.3}\text{Ga}_{0.7}\text{As}$  and GaAs of 65% we find from the relation  $\Delta E_c = 750 \text{ meV} \times X_{\text{Al}}$  and equation (1) the values for the quasi charge density  $n^+$  for the different wells as given in the last row of table 1. Of course, many more PQW with other parameters have been investigated but the scope of this report is perfectly covered by the choice of data and samples as presented here.

We now turn to a short description of the resulting

**Table 1.** Parabolic quantum wells.

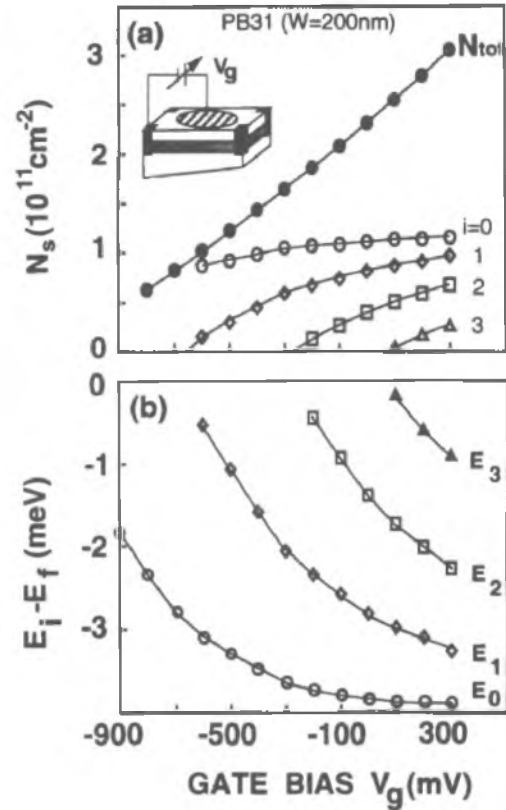
Sample	Type	X0	X1	X2	Width (nm)	$n^+$ ( $\text{cm}^{-3}$ )
PB25		0	0.1	0.3	75	$7.4 \times 10^{16}$
PB26		0	0.2	0.3	200	$2.1 \times 10^{16}$
PB31		0	0.2	0.3	200	$2.1 \times 10^{16}$
PB48		0	—	0.3	130	$7.4 \times 10^{16}$

density distribution and subband spectrum of an electron system in such a PQW. Mobile carriers that are introduced by remote doping will tend to screen the external potential of the positive quasi charge  $n^+$ , leading to a wide and nearly homogeneous electron slab. This behaviour is already intuitively clear from figures 1(c) and (d). A more detailed description, however, requires a self-consistent calculation [25]. There have been many different investigations of the self-consistency for the case of a PQW and we wish here to review only the basic results. For the case of an empty PQW the subband spectrum is the one of a harmonic oscillator with a characteristic energy

$$\hbar\omega_0 = \left( \hbar^2 \frac{8\Delta}{W^2 m^*} \right)^{1/2} \quad (2)$$

which is solely determined by the design and growth of the structure under consideration. As the well is filled, the electrons distribute themselves to form a wide layer, and the resulting conduction band profile is essentially flat over the occupied width of the PQW. Then, the single-particle subband spectrum resembles more the one of a rectangular quantum well of width  $W$ , leading to non-equally spaced subband energies. In first approximation these are given by  $E_0 n^2$ , with  $E_0$  of the order of 0.1 to 1 meV, depending on the actual sample. In other words, with decreasing carrier density and, related to this, with decreasing width of the electron layer, the subband energies increase, tending towards the equal spacing of the empty well given by equation (2).

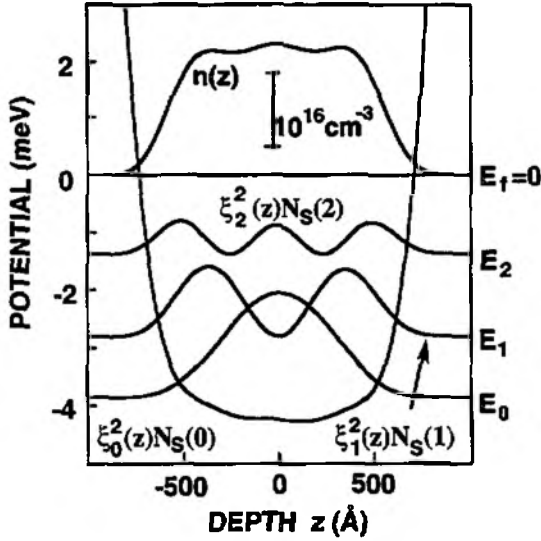
Due to the smallness of the subband energies usually more than one subband is occupied for typical carrier densities in the wells. This is demonstrated in figure 3, where we plot the results of a fully self-consistent calculation for the carrier density and the subband energies of one of the samples (PB31) investigated. In figure 3(a) the calculated carrier densities in the different electrical subbands are depicted as a function of the applied bias  $V_g$  between a metal gate electrode on top of the sample surface and the electron system in the well. The inset shows schematically the sample geometry used in all our experiments. Four indium pellets are alloyed



**Figure 3.** Result of a self-consistent calculation (symbols) for the electron densities in the different electrical subbands (a) as well as for the single-particle (Hartree) energy levels (b) of a 200 nm wide PQW as a function of the applied gate bias  $V_g$ . The interpolating curves are guides to the eye. With increasing negative bias the well becomes depleted while the upper subbands depopulate. At the same time the subband levels increase in energy. The inset shows a typical sample geometry used in our experiments.

to the electron system to form an ohmic contact. The gate electrode consists of a thin (5 nm) NiCr layer also serving as a semitransparent electrode compatible with FIR spectroscopy. In addition, on some samples a highly conducting Ag grating coupler is deposited on top of the gate electrode. This grating coupler is used to couple FIR to both inter- and intrasubband collective modes and is described in detail in section 4. One sees how with increasing negative bias  $V_g$  the total carrier density  $N_{tot}$  decreases and how at some particular gate voltages the electrical subbands become depopulated. At the same time the self-consistent Hartree potential adjusts itself such that the corresponding subband energies  $E_i$  increase as a function of decreasing carrier density as expected from the above simple arguments. This behaviour is shown in figure 3(b), where we plot the calculated subband energies  $E_i - E_f$  as a function of the gate bias. Here  $E_f$  denotes the Fermi level, which is held to be  $E_f = 0$  in the figure.

In figure 4 we show the self-consistent potential together with the calculated wavefunctions weighted by the carrier densities  $\xi_i^2(z)N_s^{(i)}$  in the subbands as a function of depth in the growth direction  $z$ . The total carrier density in this case is  $N_s = 2.4 \times 10^{11} \text{ cm}^{-2}$ ,



**Figure 4.** Self-consistently obtained Hartree potential together with the calculated wavefunctions of a PQW at high well filling. The total wavefunction represents the nearly uniform electron distribution over in this case nearly 100 nm width. At the same time the potential profile in this region is nearly flat.

corresponding to a gate bias of  $V_g = 0$  V. The total width  $W_e$  of the electron slab in this case is close to  $W_e = 115$  nm as expected from the simple relation

$$n^+ = \text{const} = \frac{N_S}{W_e}. \quad (3)$$

For this particular sample and the given carrier density three electrical subbands are occupied and the resulting total density distribution as well as the conduction band profile are nearly flat. Experimentally, the decreasing width of the slab as well as the shift of the potential minimum and thus the centre of mass of the total wavefunction can be determined by, for example, a measurement of the gate capacitance as a function of the gate bias [25]. Also, the subsequent depopulation of electrical subbands can be observed using this technique.

### 3. Long-wavelength spectroscopy on parabolically confined electron systems

Shortly after the first successful realization of remotely doped PQW some very enlightening initial experiments of Karrai and co-workers [16, 17] stimulated a lot of further experimental as well as theoretical work on this subject. Subsequently many more interesting features of parabolic quantum wells have been investigated both experimentally and theoretically. Both (magneto-)transport [26, 27] and FIR investigations [28] yielded a large number of new and interesting results which shed some light onto the understanding of many fundamental properties of low-dimensional electron systems. Here we restrict ourselves to a short description of those experiments related to the subject of the present report and refer the reader to recent review articles on, for example, the investigation of the

single-particle spectrum of a similar structure, as obtained in magnetotransport experiments [27].

#### 3.1. The generalized Kohn theorem

In a tilted magnetic field experiment similar to that of Schlesinger and co-workers and Wieck and co-workers [29] to study the resonant interaction of subband and Landau levels in a Q2DES, the authors of [16] observed that the FIR response of the electron system in a PQW is governed by a single, well defined frequency very close to the plasma frequency of a three-dimensional electron system of density  $n^+$  which by construction is given by  $\omega_0$  in equation (1). Initially, this behaviour was interpreted in terms of a successful realization of a highly mobile Q3DES. In a celebrated theoretical article, however, Brey *et al* [19] explained this result by a generalization of Kohn's theorem [18]. It states that in a purely parabolically confined electron system long-wavelength radiation only couples to the centre of mass coordinates and its motion. The reason for this is the decoupling of the centre-of-mass modes of the interacting electron gas from its internal modes. Relative coordinates and thus particularly electron-electron interactions in such systems do not affect the resonance frequency of the observed transitions. We here briefly review the basic idea of the generalized Kohn theorem which has been formulated in the recent past by numerous authors. We directly follow the work of Yip [20] and use the same formalism: suppose an electron system in a three-dimensional parabolic confining potential is subjected to a magnetic field. Putting  $\hbar \equiv 1$ , the Hamiltonian in this case in its most general form can be written as

$$H = \frac{1}{2m^*} \sum_{j=1}^N \pi_j^2 + \frac{m^*}{2} (\omega_x^2 x_j^2 + \omega_y^2 y_j^2 + \omega_z^2 z_j^2) + \sum_{(j,k)} U(r_j - r_k) \quad (4)$$

$$j = 1, 2, \dots, N \quad \pi_j = \frac{1}{i} \nabla_j - \frac{e}{c} A(r_j) \quad r_j = (x_j, y_j, z_j).$$

Here, the three-dimensional parabolic potential is parametrized in terms of the characteristic frequencies  $\omega_i$ , the influence of the magnetic field is included via  $\pi_j$ , and electron-electron interaction is included via an interaction potential  $U$  which depends only on relative coordinates  $(r_j - r_k)$ .  $N$  represents the total number of carriers in the well. Yip now introduces centre of mass and relative coordinates of the form

$$R \equiv R^{(1)} \equiv \frac{1}{N} \sum_{j=1}^N r_j \quad \Pi \equiv \Pi^{(1)} \equiv \sum_{j=1}^N \pi_j$$

$$X^{(2)} \equiv x_1 - x_2 \quad X^{(3)} \equiv x_1 + x_2 - 2x_3 \quad (5)$$

$$X^{(N)} \equiv x_1 + x_2 + \dots + x_{N-1} - (N-1)x_N$$

and similarly for  $Y^{(2)}, \dots, Y^{(N)}, Z^{(2)}, \dots, Z^{(N)}$ , and  $\Pi^{(2)}, \dots, \Pi^{(N)}$ . If the following relations are used for the

coordinates  $x_j$

$$\sum_{j=1}^N x_j^2 = \frac{1}{N} \left( \sum_{j=1}^N x_j \right)^2 + \frac{1}{N} \sum_{1 \leq i, j \leq N} (x_i - x_j)^2 \quad (6)$$

and equivalently for  $y_j$ ,  $z_j$  and  $\pi_j$ , it can be shown that now the total Hamiltonian can be separated into two terms  $H = H_{\text{CM}} + H_{\text{rel}}$ , where  $H_{\text{CM}}$  is given by

$$H_{\text{CM}} = \frac{1}{2Nm^*} \Pi^2 + \frac{Nm^*}{2} \left( \omega_x^2 X^2 + \omega_y^2 Y^2 + \omega_z^2 Z^2 \right) \quad (7)$$

and the term  $H_{\text{rel}}$  is more complicated but only involves the relative coordinates and momenta. Since the external magnetic field is assumed to be uniform across the sample,  $A(r_i)$  is a linear functional and thus

$$\Pi = \frac{1}{i} \nabla_R - \frac{Ne}{c} A(R).$$

It follows that  $[H_{\text{CM}}, H_{\text{rel}}] = 0$  and  $|\Psi\rangle = |\Psi_{\text{CM}}\rangle |\Psi_{\text{rel}}\rangle$ .

The centre of mass and the relative motion thus separate and the eigenfrequencies  $|\Psi_{\text{CM}}\rangle$  are identical to those of a single electron in the bare parabolic confining potential. The interaction of the electron system with the optical field of the long-wavelength FIR is expressed via a uniform, time-dependent perturbation

$$H_1 = - \frac{e}{mc} \sum_j \pi_j A_1 \quad A_1 \neq A_1(r_j) \quad (8)$$

which leads to

$$H_1 = - \frac{e}{mc} \Pi A_1 \Rightarrow H_1 |\Psi\rangle = H_1 |\Psi_{\text{CM}}\rangle. \quad (9)$$

In other words, in a purely (one-dimensional) parabolic confining external potential only the frequency  $\omega_0$  given by equation (2) is observed in a FIR experiment, independent of the choice of the electron-electron interaction. This mode is of intersubband type and represents a sloshing of the whole electron system, represented by its centre of mass (CM) in the external parabolic potential. Meanwhile, many different experiments including those on QIDES and QODES have proved the validity of this statement [3]. It was shown that the generalization of Kohn's theorem indeed holds and that the observed intersubband-like resonance frequency of an electron system in a parabolic confining potential is independent of electron-electron interactions and thus the actual number of carriers in the well.

### 3.2. Imperfect parabolic quantum wells

So far we have been dealing with electrons in ideal parabolic confining potentials. Here, the generalized Kohn theorem is directly applicable. No real system, however, can be regarded as being completely ideal. First, no artificial potential is infinitely deep; in other words, at some finite energies there must be a cut-off where parabolicity is no longer maintained. Secondly, there might be some unintentionally induced non-parabolic terms in the potential which are related to some

imperfection during the growth of the structures. Even more serious is the situation for quantum wires and dots where the parabolic model is certainly only valid in first order. Thus, it is highly desirable to gain some insight into the behaviour and FIR response of electron systems which are confined in 'imperfect' parabolic potentials. As far as MBE-grown quantum wells are concerned we have the possibility to tailor any kind of desired band structure artificially and thus are able to intentionally induce a certain degree of non-parabolicity [9, 30]. These structures may then also serve to a better understanding of many properties of quantum dots and wires where the confining potential is not exactly known *a priori*. Early experimental results on such samples, which will be addressed in section 5, have indeed triggered a lot of valuable theoretical work on the subject of imperfect PQW such that we now are in the pleasant situation of also having some knowledge about the properties of nearly parabolic confining potentials, where Kohn's theorem is no longer strictly applicable. Most interesting is the fact that in such systems symmetry-forbidden transitions can be observed which occur due to non-local interactions in the electron system. Such calculations have been performed by using either a hydrodynamic approach [31] or a fully self-consistent calculation in a random phase approximation (RPA) framework [32–35]. In section 5 we shall directly apply the results of the existing theories to our experimental findings and also give more details of the models that have been developed and used in the past.

### 3.3. Finite wavevector

A very interesting subject of investigation is the collective excitation spectrum of electron systems at finite wavevector  $q$ . Here, the coupling of FIR to intrasubband plasmons also becomes possible [11, 12, 36, 37]. These are collective modes of charge density oscillation with surface excitation character. For Q2DES there exists a whole library of literature on those modes which has proved invaluable to the understanding of the collective spectrum of low-dimensional systems [2]. More recently, the collective excitation spectrum of QIDES has also attracted very much attention. Demel and co-workers [5] succeeded in the observation of so-called one-dimensional plasmons which represent a charge density oscillation along the free direction of a quantum wire. A very characteristic magnetic field dispersion of these modes has been observed which indicates the edge-excitation character of such collective modes. On the other hand, the resonant coupling between intra- and intersubband collective excitation is also of great interest since here much information on the dynamic behaviour of low-dimensional electron systems can be obtained. Such coupling was first observed by Oelting and co-workers [38] for a 2DES in an elegant experiment after it has been theoretically predicted by Das Sarma [39]. More recently Li and Das Sarma [40] as well as Gold and Ghazali [41] focused on the interaction of 1D intersubband resonances with 1D intrasubband



plasmons. Here a resonant interaction is more likely than in the 2D case, since for typical sample parameters both modes are energetically of approximately the same size.

For a QW of finite width a strict separation of surface and bulk character of the plasma modes is no longer possible once the thickness of the electron slab becomes comparable with the inverse of the wavevector of the excitation. Then strong mode coupling occurs, leading to a characteristic dispersion of the modes. In a PQW one has the possibility of changing both the carrier density in the well and the effective width of the electron slab, which makes it a favourable subject for very detailed investigation of these interesting facts.

#### 4. Experimental remarks

All our experiments are performed in transmission using a rapid scan Fourier transform spectrometer (Bruker IFS 113) connected to a low-temperature ( $T \geq 2$  K) and high-magnetic-field ( $B \leq 15$  T) system. The samples under investigation are mounted on a sample stage centred in the superconducting solenoid and providing the possibility of tilting the sample with respect to the magnetic field direction ( $0 \leq \Theta \leq \pi/2$ ). Usually, unpolarized FIR is normally incident, so that we can investigate all configurations between Faraday ( $\Theta = 0$ ) and Voigt ( $\Theta = \pi/2$ ) geometry. A thin NiCr layer on top of the sample serves as a semitransparent gate electrode and In pellets are alloyed to the electron system to provide ohmic contacts. Application of a negative bias  $V_g$  between the gate electrode and the electron system tends to deplete the well as already mentioned in section 2. Experimentally, we determine the relative change in transmission  $-\Delta T/T = (T(0) - T(N_s))/T(0)$  which is proportional to the real part of the effective conductivity  $\tilde{\sigma}(\omega)$  of the system, depending on the actual polarization used in the experiment [42].  $T(0)$  is the transmission of the sample with the well being completely depleted,  $T(N_s)$  the transmission at finite carrier densities. A silicon composite bolometer held at  $T = 2$  K is used to detect the transmitted radiation. On some samples silver grating couplers have also been prepared using either standard optical lithography or holographic techniques for the shorter-period gratings. The periodicities of the grating couplers used in our experiments vary between  $a = 6 \mu\text{m}$  and  $a = 0.8 \mu\text{m}$  to provide both the necessary  $z$  component of the FIR to couple directly to intersubband-like excitations as well as the finite  $q = 2\pi/a$  for the surface (intrasubband) plasmon experiments [2]. The sample substrate is wedged to about  $3^\circ$  to avoid disturbing interference effects on the transmission spectra.

#### 5. Experimental results and discussion

##### 5.1. Ideal parabolic quantum wells

In this section we shall concentrate on a review of the FIR response of what we call 'ideal' PQW, i.e. quantum

wells with no intentionally induced deviation from parabolicity. Such samples are represented by PB26, a 200 nm wide PQW, where the Al mole fraction was varied during growth between  $x = 0$  in the centre to  $x = 0.2$  at the edges and with additional vertical sidewalls up to  $x = 0.3$ , and a 130 nm wide PQW (PB48) with  $x$  going from zero to  $x = 0.3$  at the edges. For PB26 this corresponds to a curvature of the parabola which simulates a positive background charge of  $n^+ = 2.1 \times 10^{16} \text{ cm}^{-3}$ , leading to an expected characteristic energy of  $\hbar\omega_0 = 5.8 \text{ meV} \simeq 47 \text{ cm}^{-1}$ . For PB48 we expect from growth  $\hbar\omega_0 = 10.7 \text{ meV} \simeq 86 \text{ cm}^{-1}$ . The sheet carrier density of both samples at  $V_g = 0$  V is about  $N_s = 3 \times 10^{11} \text{ cm}^{-2}$ , the electron mobility for both samples is of the order of  $\mu = 15 \text{ m}^2 \text{ V}^{-1} \text{ s}^{-1}$ .

We first present the results of tilted magnetic field experiments, i.e. where coupling to the intersubband-like mode is achieved by a resonant coupling of the cyclotron resonance (CR)  $\omega_c = eB/m^*$  to the sloshing mode of the centre of mass  $\omega_0$ . For an ideal PQW, due to Kohn's theorem only this mode couples to the CR in a tilted magnetic field [19]. In this case the theoretical description of the interaction is particularly simple and can be treated like the coupling of two harmonic oscillators of frequencies  $\omega_0$  and  $\omega_c$ . The tilt angle enters the problem via the normal and parallel projections of the CR, namely  $\omega_{c,x} = \omega_c \sin \Theta$  and  $\omega_{c,z} = \omega_c \cos \Theta$ . This problem was treated originally by Maan [43] and independently by Merlin [44]. The result is the occurrence of a mode anticrossing between the two resonances if the magnetic field is varied such that  $\omega_0$  and  $\omega_c$  energetically degenerate. The resonance positions in this case are given by the simple expression

$$\omega_{\pm} = \sqrt{\frac{1}{2}(\omega_c^2 + \omega_0^2) \pm \frac{1}{2}\sqrt{\omega_c^4 + \omega_0^4 + 2\omega_0^2(\omega_{c,x}^2 - \omega_{c,z}^2)}}. \quad (10)$$

For harmonic oscillators the resulting gap due to the anticrossing is solely determined by the tilt angle, whereas for more complicated potential profiles in general the appropriate matrix elements are involved. The oscillator strengths of both CM modes are also very easily calculated

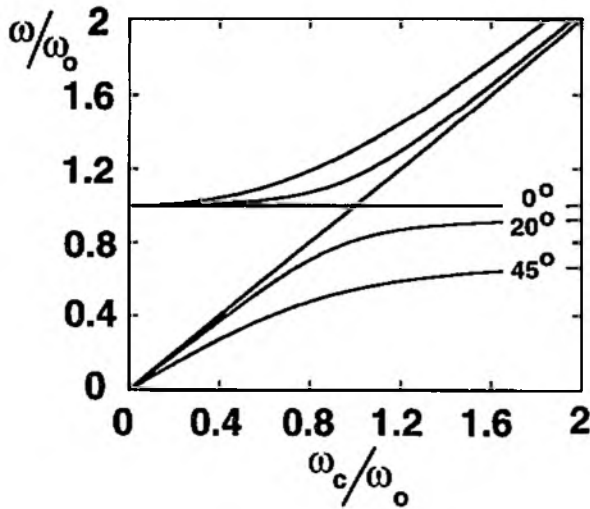
$$\begin{aligned} f_+ &= \frac{1}{2}(f_+^{(y)} + f_+^{(x)}) \\ &= \frac{1}{2}\left(\sin^2 \alpha + \frac{(\omega_{c,x} \cos \alpha + \omega_{c,z} \sin \alpha)^2}{\omega_+^2}\right) \\ f_- &= \frac{1}{2}(f_-^{(y)} + f_-^{(x)}) \\ &= \frac{1}{2}\left(\cos^2 \alpha + \frac{(\omega_{c,y} \sin \alpha + \omega_{c,z} \cos \alpha)^2}{\omega_-^2}\right) \end{aligned} \quad (11)$$

where the angle of rotation  $\alpha$  is given by

$$\tan 2\alpha = \frac{2\omega_{c,y}\omega_{c,z}}{(\omega_0^2 + \omega_{c,y}^2 - \omega_{c,z}^2)}.$$

For low magnetic fields  $\omega_-$  has the character of the cyclotron resonance, whereas  $\omega_+$  represents an intersubband-like mode. The situation is reversed for high magnetic fields, and in the magnetic field regime where both modes are energetically degenerate, they exchange



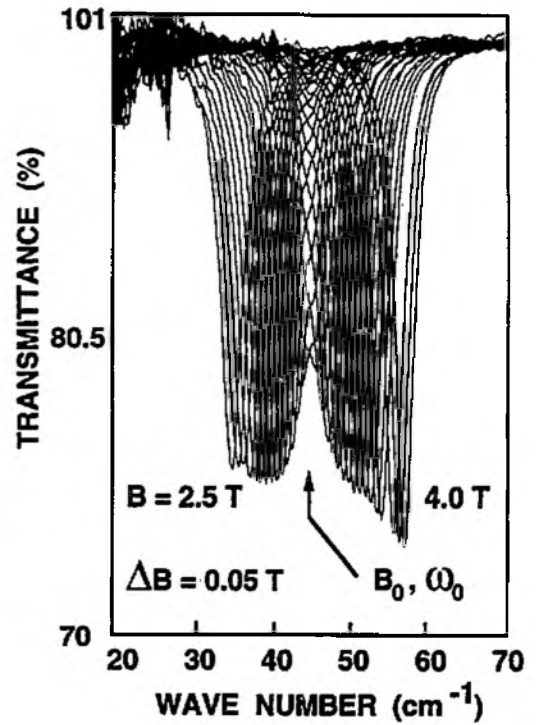


**Figure 5.** Calculated resonance positions of the modes  $\omega_+$  and  $\omega_-$  according to equation (10) for a parabolic well subjected to a tilted magnetic field. Due to mode coupling the degeneracy between the two modes is lifted as soon as the tilt angle  $\Theta$  between the sample normal and the magnetic field direction is non-zero. For two coupled harmonic oscillators, the resulting gap between the two lines is solely determined by the tilt angle.

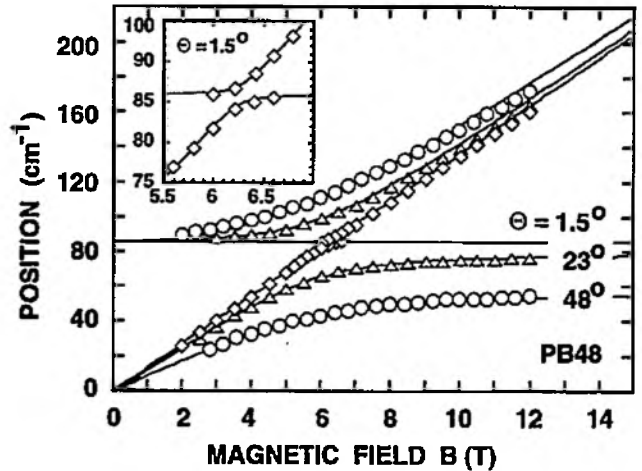
oscillator strength. The results of equations (10) and (11) are depicted in figure 5, where we plot the resonance positions of  $\omega_{\pm}$  as a function of the total magnetic field in units of  $\omega_0$  and tilt angles of  $\Theta = 0, 20$  and  $45^\circ$ . For  $\Theta \neq 0$ , the degeneracy between the two modes is lifted, resulting in a characteristic anticrossing of the two lines.

A typical example for the mode anticrossing at a very small tilt angle is given in figure 6, where we show a series of observed cyclotron resonance lines for sample PB26 at different magnetic fields between  $B = 2.5$  T and  $B = 4.0$  T using small magnetic field steps of  $\Delta B = 0.05$  T. Clearly one observes the region of interaction resulting in a strong modulation of the CR lineshape. At  $B = B_0 \approx 3.5$  T and  $\omega = \omega_0 \approx 46$   $\text{cm}^{-1}$  there is a sharp dip in the envelope of the spectra, reflecting the exchange of oscillator strength and the anticrossing of both lines involved. The small tilt angle in this case is only given by the wedge angle of the sample, namely  $\Theta \approx 3^\circ$ . Even here, clearly an interaction between the CR and the sloshing mode of the centre of mass of the electron system is detectable, although the two modes are not yet strictly separated.

In figure 7 we depict the result of a tilted field experiment on sample PB48 for three different tilt angles. The symbols represent the extracted resonance positions and the full curves are the result of a calculation according to equation (10). For all three experiments the same parameters have been used as given in the inset of the figure. The agreement between our experimental results and the simple model calculation is nearly perfect for all three angles investigated. The small but reproducible deviations between theory and experiment at higher magnetic fields are due to band non-parabolicity, which has not been included in the calculation.

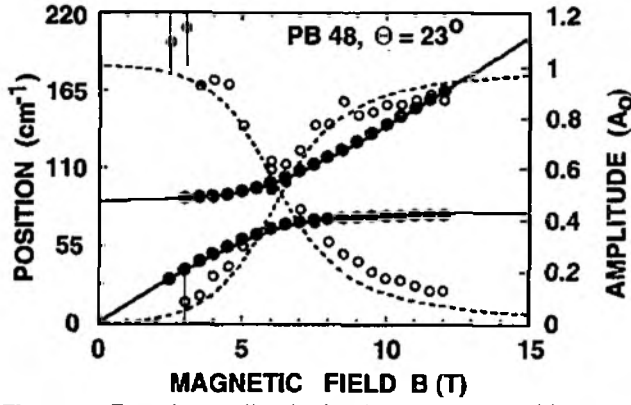


**Figure 6.** Experimentally obtained spectra of the cyclotron resonance in a PQW in a tilted magnetic field. The tilt angle in this case is very small ( $\Theta = 3^\circ$ ) such that a splitting of both lines according to equation (10) is not yet achieved. Nevertheless, a sharp dip in the envelope of the spectrum indicates the region of anticrossing between the two lines and allows for an exact determination of the resonance condition.



**Figure 7.** Experimentally obtained resonance positions for three different tilted field experiments as a function of the total magnetic field strength  $B$ . With increasing tilt angle the mode anticrossing becomes more pronounced, leading to a well defined separation of the two lines. The full curves are the result of a calculation according to equation (10) using  $m^* = 0.07m_0$  and  $\hbar\omega_0 \approx 86$   $\text{cm}^{-1}$  for all three measurements. Thus, the experimental data are perfectly described within the simple model of two coupled harmonic oscillators.

In figure 8 we show the result of the tilted field experiment for PB48 at a tilt angle of  $\Theta = 23^\circ$  together with the amplitude of the observed resonances which has

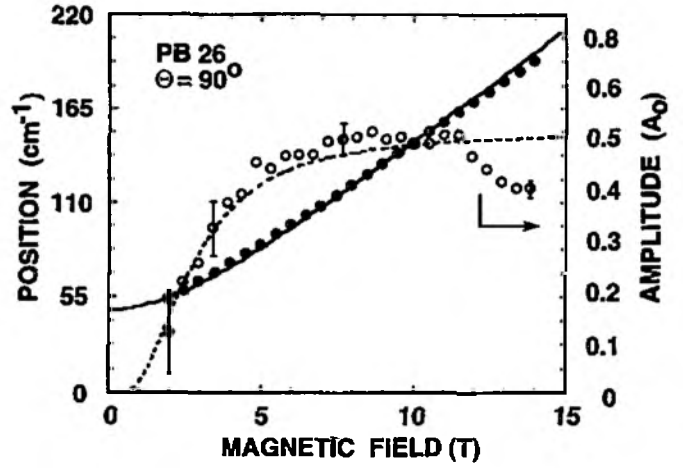


**Figure 8.** Experimentally obtained resonance positions (full symbols) of a tilted field experiment at  $\Theta = 23^\circ$  together with the result of a calculation (full curves) according to equation (10). Also shown are the extracted intensities (open symbols) normalized to the one obtained in a normal magnetic field, which are proportional to the oscillator strength if the linewidth does not change significantly over the magnetic field range shown. The broken curves are the result of equation (11), assuming unpolarized far-infrared radiation and normal incidence.

been normalized to the one of the CR in perpendicular magnetic fields. Taking the width of the resonance fixed, which is justified here, this quantity is proportional to the oscillator strength. The broken curves represent the prediction in the simple harmonic oscillator picture as given in equation (11). At low magnetic fields in particular there exists a quite large scatter around the expected value for the oscillator strength. This we believe is caused by effects arising from the population and depopulation of different subbands in the system: the different spatial extent of the wavefunctions in different subbands leads to the occurrence of an 'artificial non-parabolicity' [7], resulting in a superposition of different CR lines which then may complicate the proper evaluation of the oscillator strength. Also, the effective electron mass  $m^*$  turns out to be a function of position in the well. These effects, as well as those of subband depopulation and intersubband scattering, however, are beyond the scope of the present report and will be discussed elsewhere.

Under the extreme condition of an in-plane magnetic field ( $\Theta = 90^\circ$ , Voigt geometry), only  $\omega_+$  is observable. The electrical and the magnetic confinements act in the same direction and the CR hybridizes with the oscillation in the bare potential as represented by  $\omega_0$ . For small magnetic fields, electrical quantization is stronger than magnetic quantization and the observed resonance frequency is close to  $\omega_0$ . For higher magnetic fields magnetic quantization becomes dominant and the observed resonance approaches  $\omega_c$ . In a well with perfect parabolicity this resonance is a discrete excitation that is split off from the continuum of inter-Landau level transitions by collective polarization effects. The resonance position and the oscillator strength of the hybrid mode are then given by

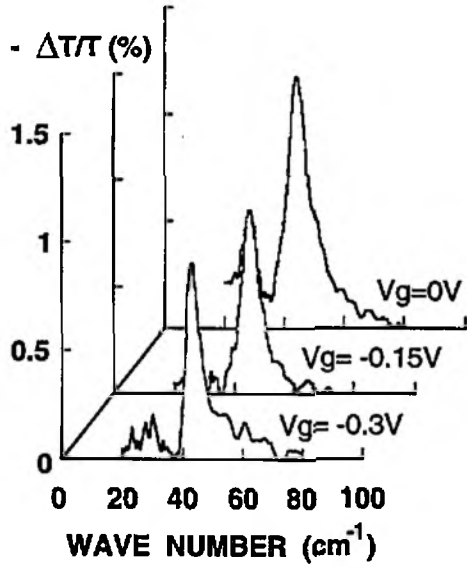
$$\omega_+^2 = \omega_c^2 + \omega_0^2 \quad \text{and} \quad f_+^{(x)} = \frac{1}{2} \frac{\omega_c^2}{\omega_0^2 + \omega_c^2}. \quad (12)$$



**Figure 9.** The analogue experiment of figure 8 in Voigt-geometry. Here, the magnetic field is directed along the plane of the pqw, which leads to a complete hybridization of both the cyclotron resonance and the sloshing intersubband-like mode of the pqw that obeys Kohn's theorem. Full symbols and the full curve represent the extracted and calculated resonance positions as a function of the in-plane magnetic field. Open symbols and the broken curve depict the intensity (oscillator strength) as extracted from our experiment and calculated using equation (12). The origin of the discrepancies between the oscillator strength as obtained experimentally and theoretically is not known, to date.

Here, it is interesting to note that exactly the same magnetic field dispersion is expected and in fact observed for quantum wires (Q1DES) with parabolic confinement in a perpendicular magnetic field [3], so that our pqw in Voigt geometry may serve as a perfect model system for the investigations of such Q1DES. The result of such an experiment on a pqw is shown in figure 9, where we plot the extracted resonance position together with the amplitude of the line for sample PB26. Again, it has been normalized to that of the CR in Faraday geometry. The symbols represent the experimental results, and the curves are the result of the calculation according to equation (12). The origin of the large deviation of the measured oscillator strength from the expected value above  $B = 12$  T is not yet known. For the geometry of this experiment and the related FIR polarization the oscillator strength vanishes for  $B \rightarrow 0$ . Using a grating coupler technique, however, we are able to follow the resonance down to  $B = 0$ .

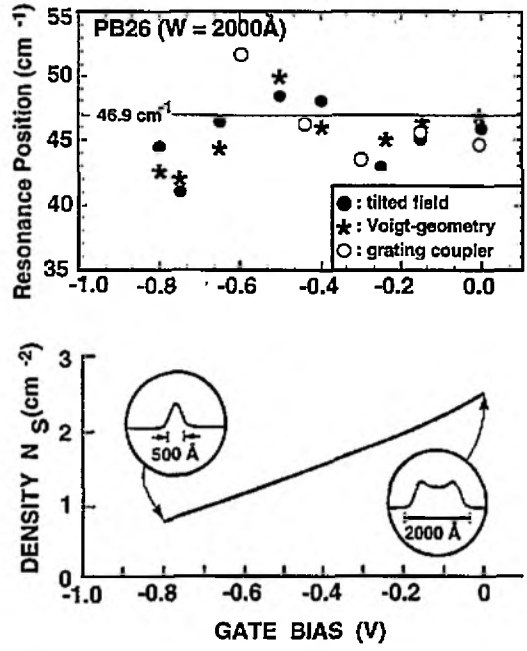
An example of such a direct observation of the intersubband-like sloshing mode of a pqw [9] is given in figure 10. Here, we plot the result of a grating coupler-induced resonance for sample PB26 for three different gate voltages  $V_g$  and correspondingly three different carrier densities in the well. To induce longitudinal electric components in the FIR radiation that are transmitted through the sample parallel to the growth direction we use a 70 nm thick Ag grating coupler of periodicity  $d = 6 \mu\text{m}$  that is deposited in addition to the semitransparent NiCr gate electrode on top of the sample. Although the carrier density in the well is changed from  $N_s = 2.5 \times 10^{11} \text{ cm}^{-2}$  at  $V_g = 0$  V down to  $N_s = 1.6 \times 10^{11} \text{ cm}^{-2}$  at  $V_g = -0.3$  V, the



**Figure 10.** Grating-coupler-induced intersubband-like resonance (sloshing mode) of a 200 nm wide PQW (PB26) for three different gate voltages  $V_g$  or carrier densities  $N_s$ , respectively. Although the density has been changed from  $N_s = 2.5 \times 10^{11} \text{ cm}^{-2}$  down to  $N_s = 1.6 \times 10^{11} \text{ cm}^{-2}$  the resonance position does not change, in agreement with Kohn's theorem. The spectra have been taken at zero magnetic field.

position of the grating coupler-induced resonance is not changed. The decrease of the carrier density, however, is reflected in a reduced oscillator strength, as can be seen in figure 10. The exact amplitude of the observed resonance depends not only on the dynamic conductivity  $\sigma_{xx}(\omega)$ , and thus on the carrier density  $N_s$ , but also on the efficiency of the grating coupler used in the experiment. For this reason, we cannot directly compare different spectra obtained for different samples and grating couplers.

The resonance positions of the intersubband-like sloshing mode in sample PB26 as obtained from all the different experimental techniques are summarized in figure 11 as a function of the gate bias  $V_g$ . Different symbols represent the results of different experiments as given in the inset. The lower panel of figure 11 shows the change in width of the electron layer confined in the parabolic well as a function of gate bias. Although this width is changed by approximately a factor of four, no significant change of the resonance position is observed. However, there is a small but reproducible scatter of the data around the expected values of  $\omega_0 \approx 46.9 \text{ cm}^{-1}$  which is indicated by a thin horizontal line in the figure. Within the resolution of the experiments this scatter is independent of the way that it is obtained, indicating an intrinsic origin. We believe that it is the result of a sensitive test of the local curvature of the PQW around the potential minimum. Such small changes in the curvature of an MBE-grown PQW cannot be completely excluded and have in fact been observed in different experiments and direct measurements [45]. Application of a negative gate bias shifts the potential minimum deeper into the sample such that a specific gate bias is



**Figure 11.** Resonance energy of the absorption of a PQW as obtained using three different techniques as indicated in the inset versus the gate bias or the carrier density, respectively (top). The thin horizontal line indicates the natural frequency of the respective well (PB26) as expected from the growth alone. There is a small but reproducible scatter of the experimentally obtained positions around the expected value, which we attribute to a sensitive test to the local curvature of the well. The bottom panel sketches the change in carrier density or equivalently the width of the electron slab with gate bias [22].

related to a possible slightly different local curvature. This assumption appears to be justified by the fact that the scatter becomes larger once the width of the electron slab is reduced: the wider the electron system, the less important short-range fluctuations of the actual curvature of the PQW become and vice versa. Since the positions of the resonances crucially depend on the actual shape of the bare potential, small deviations from a constant curvature have a large impact on the resonance positions.

In a theoretical analysis of the spectrum of 'imperfect parabolic quantum wells', Brey and co-workers [32] studied the influence of small additional quartic terms  $\Delta_q$  in the potential as a measure for deviations from parabolicity. They found that such a correction is quite effective in shifting the absorption line. For example, a positive  $\Delta_q$  causes a convex parabolic correction to the nearly uniform charge distribution produced by the parabolic potential alone. This leads to an additional confinement of the carriers and thus to an increase of the resonance position. A negative  $\Delta_q$ , however, induces an additional concave parabolic component, leading to a spreading of the charge as compared with the ideal parabola and thus to a reduction of the resonance position. A rough estimate yields that a shift of the absorption line by 5% can be caused by quartic contributions to the potential of the order of  $\Delta_q/\Delta_p \approx 0.1$  where  $\Delta_p$  denotes the parabolic coefficient of the potential. In other words, although we cannot state

definitely that the observed resonance position does not depend on the gate bias  $V_g$ , we have strong indication that it does not depend on the actual carrier density in the well in accordance with Kohn's theorem.

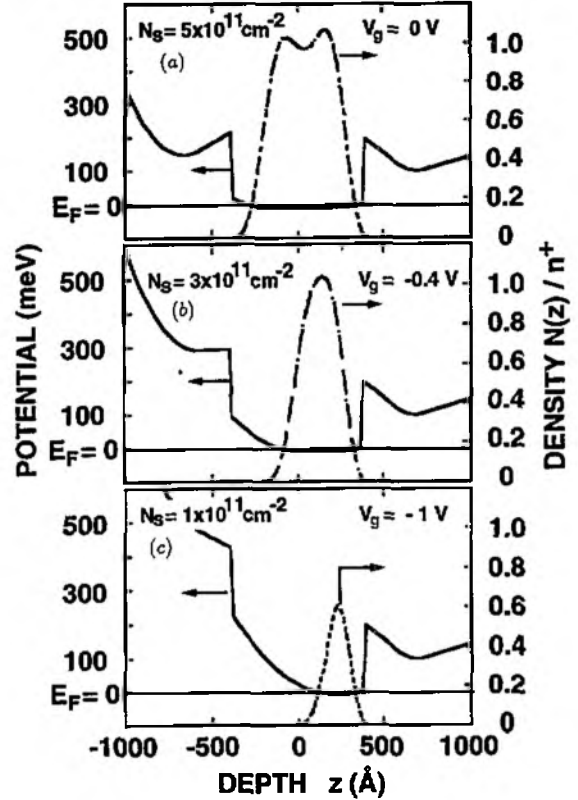
### 5.2. Imperfect parabolic quantum wells

In the last section we saw that for electron systems confined in purely parabolic potentials the generalized Kohn theorem is applicable. Purely parabolic confining potentials, however, do not exist in reality. There are two major sources for deviations from parabolicity:

- (i) No real potential is infinitely deep. For the special case of PQW this is equivalent with the finite height of the AlGaAs barriers enclosing the quantum well. In other words, the finite size of the system under consideration in principle violates the theorem. We will refer to this source of deviation as finite size effects.
- (ii) There might be some unintentional small deviations in the curvature of the MBE-grown parabola. In first-order approximation those deviations may be considered in a series expansion of the confining potential. These effects will be referred to as higher-order effects.

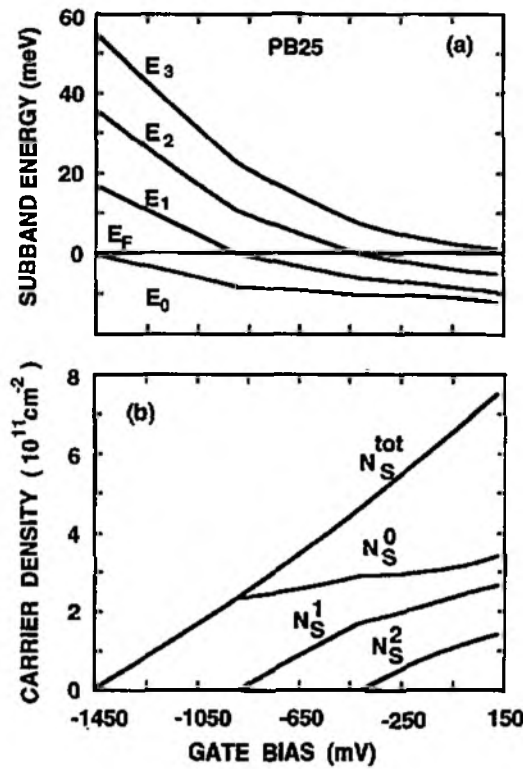
Both (i) and (ii) are not only restricted to the case of an MBE-grown PQW: finite size effects certainly occur in all kind of man-made potential profiles. The question only reduces to a comparison of relevant energy scales, like, for example, the ratio of the Fermi energy to the height of the potential. Effects arising from higher orders in the confining potential (ii) are the most universal approach to model deviations from parabolicity. Self-consistent calculations for quantum wires [46] show that, independent of the way of preparing such wires (electrostatically or by deep mesa etching), the resulting confining potential is somewhere in between a parabola and a rectangular quantum well. Such a potential then can be modelled by a parabola plus additional higher-order terms.

To study the influence of deviations from perfect parabolicity, and thus from the validity range of the generalized Kohn theorem, parabolic quantum wells seem to be a nearly perfect tool. Unlike the case of quantum wires or dots the external confining potential can be tailored in a very precise and controlled way during the growth of the structure. Moreover, optical experiments on *imperfect parabolic quantum wells* can yield information not only about the extent to which the confining potential deviates from perfect parabolicity, but also—for small deviations—about the forbidden excitation of an ideal system [31]. Here we present the experimental results obtained in a structure (PB25) where we intentionally induced a certain degree of non-parabolicity to study its influence on the FIR spectrum. Moreover, the sample has been designed such that we can electrically tune the degree of deviation and switch between different limiting cases. The sample is a nominally 75 nm wide PQW with  $\Delta = 75$  meV, having vertical sidewalls which are 150 meV high. The curvature of PB25 is chosen such that we expect the bare harmonic oscillator



**Figure 12.** Results of a self-consistent calculation for the sample PB25 ( $W = 75$  nm,  $\Delta = 75$  meV). Both the self-consistent potential and the resulting charge distribution  $N(z) = \sum_i N_s |\xi_i|^2$  are depicted as functions of depth  $z$ . The centre of the PQW is located  $z = 0$ . Note the considerable shift of the electron distribution with increasing negative gate bias. In (a) we show the situation for the completely filled well, (b) depicts intermediate filling, whereas in (c) the well is nearly depleted and strongly asymmetric [9].

frequency to be  $\omega_0 \approx 86$   $\text{cm}^{-1}$ . The result of a self-consistent potential and subband calculation for this sample is shown in figure 12, where we plot the self-consistent potential together with the total wavefunction as a function of depth for three different gate voltages or carrier densities in the well. The gate electrode is situated at the left-hand side, the substrate at the right-hand side. In figure 12(a), the well is nearly completely filled at a carrier density close to  $N_s = 5 \times 10^{11} \text{ cm}^{-2}$  at  $V_g = 0$  V. Here, the vertical sidewalls will certainly influence the finite size effects as mentioned above. For intermediate carrier densities or well fillings the wavefunction is located in the purely parabolic part of the confining potential and we expect the sample to behave like a 'normal' PQW. This situation is shown in figure 12(b) for a carrier density of  $N_s = 3 \times 10^{11} \text{ cm}^{-2}$  at  $V_g = -0.4$  V. For very low carrier density or very negative gate bias (figure 12(c)) close to total depletion of the well we expect that the resulting self-consistent potential looks more like a half-parabola, thus containing strong higher-order coefficients in the curvature. In this case only one electrical subband remains occupied, leaving the system in the electrical quantum limit. In figure 13 we depict the single-particle subband energies and the resulting subband

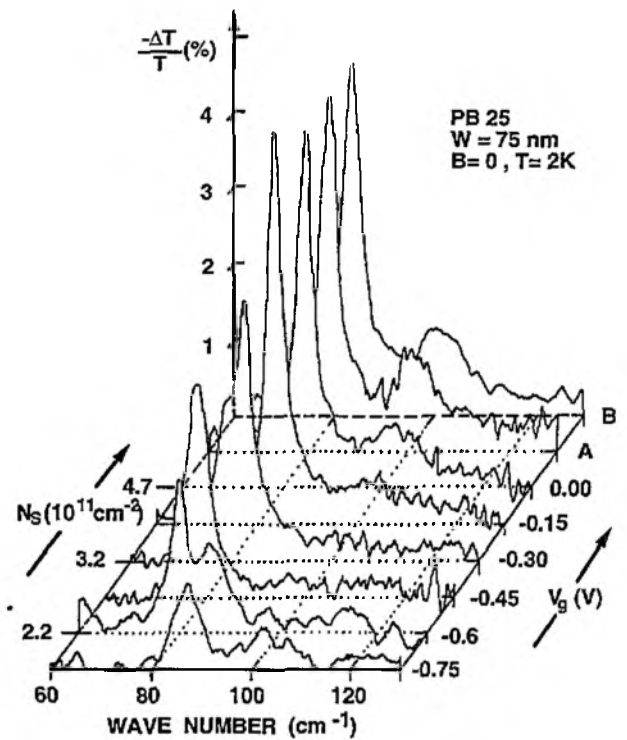


**Figure 13.** Self-consistent subband energies (a) and carrier densities (b) for the sample PB25. At high well filling up to three electrical subbands are occupied.

population for sample PB25 as obtained from self-consistent calculations. This calculated single-particle band structure and subband filling has been shown before to be very close to reality, since in various (magneto-) transport experiments we can directly compare it with our experimental results [27].

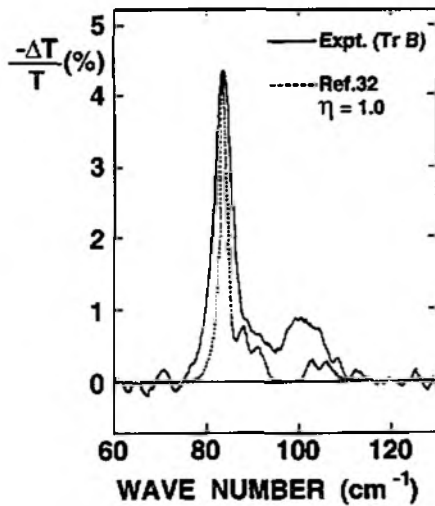
An experimental spectrum for this ‘imperfect’ sample as obtained using the grating coupler technique is shown in figure 14. Here, we plot the relative change in transmission versus FIR frequency for different gate voltages  $V_g$ . Capacitance-voltage measurements on the same sample reveal a threshold voltage of  $V_{Th} = -1.2$  V for complete depletion. Trace A has been recorded after illuminating the sample at  $V_g = 0$  V for some seconds with an IR light emitting diode, thus increasing the carrier concentration via the persistent photoeffect. Trace B is taken at a gate bias of  $V_g = +0.6$  V and after illumination, which further increases  $N_s$ . The exact values for the densities at A and B, however, have not been determined in the experiment. From an analysis of the oscillator strength of the resonance,  $N_s(B)$  is estimated to be about  $6 \times 10^{11} \text{ cm}^{-2}$ . As can be seen from the figure, in this special sample the electron system not only absorbs at the frequency of the bare harmonic potential, but side lines appear in the spectrum. The main line, however, remains quite unaffected throughout the range of carrier densities shown, indicating the rigidity of Kohn’s theorem even for this highly perturbed sample.

The influence of non-parabolic contributions to the well potential, as listed above, has recently been discussed in considerable detail by Brey and co-workers [32]. They



**Figure 14.** Experimentally obtained grating-coupler-induced spectra for sample PB25. The relative change in transmission is shown for different gate voltages  $V_g$  and carrier densities  $N_s$ . Traces A and B have been taken after a short illumination of the sample ( $V_g(A) = 0$  V,  $V_g(B) = +0.6$  V), which still increases  $N_s$  in the well. In limits of both high and low electron concentration deviations from the harmonic oscillator picture are observed, manifesting themselves in the occurrence of additional lines [9].

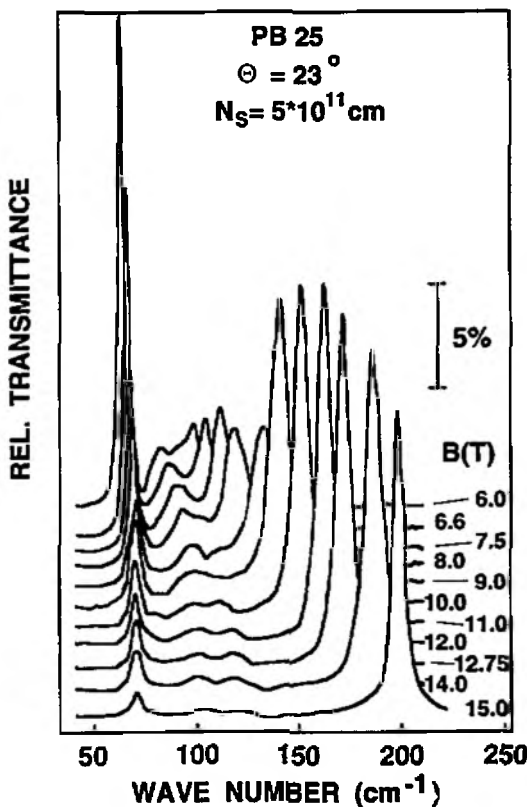
calculate the IR absorption of ‘imperfect’ parabolic wells using the local density approximation for a PQW similar to the ones we use in our experiments. For comparison, in figure 15 we replot the result of Brey *et al* for a completely filled well, where finite size effects become important, together with trace B from figure 14. The amplitude of the main line of the calculation has been normalized to the experimental one. Clearly all essential features of the experiment are reproduced in the calculation, although the linewidths and the exact position of the satellite structure differ slightly. This is believed to be caused by the fact that the parameters of the sample assumed in the calculation are not exactly identical with ours and that a phenomenological scattering time  $\tau$  has been used in the calculation. According to Brey *et al*, for a well-filling  $\eta = N_s/(n^+ W) \approx 1$ , the perturbation has two main effects on the IR absorption of a PQW. First, the additional confinement leads to a slight shift of the main absorption line to a higher frequency, and secondly, small satellites begin to appear, reflecting the coupling of light to the internal oscillations of the electron system. As can be seen in figure 14, this crossover is clearly discernible from our data. At high  $\eta$  two lines are clearly observed. The one of smaller oscillator strength and of higher frequency disappears with decreasing  $N_s$ . At intermediate



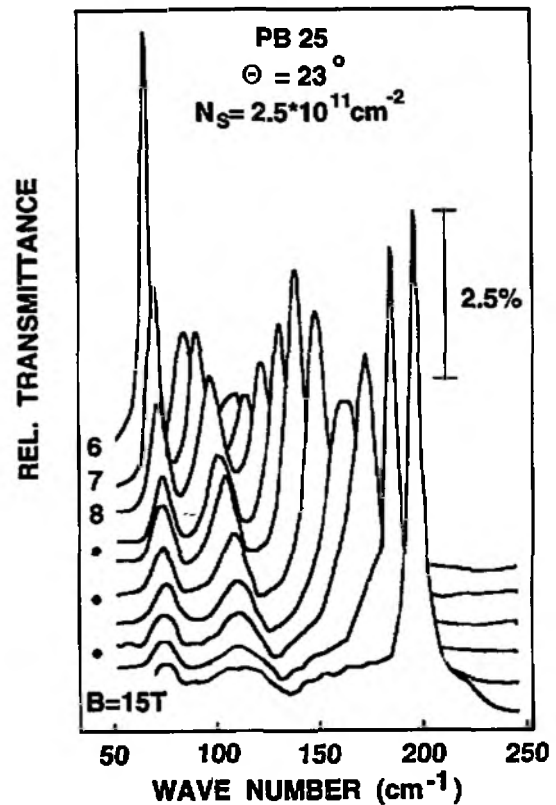
**Figure 15.** Comparison of the experimentally obtained resonances of trace B in figure 14 with those calculated by Brey *et al* for a completely filled pqw. The sidelines are due to internal oscillations of the electron system caused by the finite width of the well. All essential features of the experiment are reproduced in the calculation of the far-infrared absorption. The deviations are believed to occur owing to differences in the sample parameters in both cases and the uncertainty of the exact filling factor  $\eta$  in the experiment [9].

densities only one resonance is observed until at low  $N_S$  the system begins to feel the strong deformation of the potential associated with the vertical confining sidewall (cf figure 12(c)). Here, the model of the harmonic oscillator is certainly not valid any more, and as a consequence additional resonances appear.

Experiments in a tilted magnetic field confirm this observation. Here, we make use of the effect of a certain 'contrast enhancement' in such types of measurements: Although the oscillator strengths of the additional lines may be quite small compared with the main line, their existence may lead to a resonant interaction between these modes and the cyclotron resonance similar to that for a perfect well. Typical examples of such tilted field experiments for sample PB25 at different gate bias  $V_g$  and carrier density  $N_S$ , respectively, are given in figures 16 to 19 for a series of magnetic fields. Here, we depict a series of FIR spectra obtained for a tilt angle of  $\Theta = 23^\circ$  between the sample normal and the magnetic field direction. The spectra shown cover the upper magnetic field range between  $B = 6$  T and  $B = 15$  T. The most remarkable feature here is the occurrence of additional small lines in the gap between the CR-like and the ISR-(intersubband-like plasmon)like modes, which are not present in ideal parabolic wells (cf figures 7, 8 and 9). The more the well is disturbed from ideal parabolicity,



**Figure 16.** Experimentally obtained spectra for sample PB25 at high well filling in tilted magnetic fields  $6\text{ T} \leq B \leq 15\text{ T}$ . The tilt angle between the sample normal and the direction of the magnetic field is  $\Theta = 23^\circ$ . Due to the intentionally induced deviations from 'ideal parabolicity' new lines which are not present in an 'ideal' pqw are observed within the gap between the two centre of mass modes  $\omega_+$  and  $\omega_-$ .



**Figure 17.** Experimentally obtained spectra for sample PB25 at intermediate well filling in tilted magnetic fields  $6\text{ T} \leq B \leq 15\text{ T}$ . Note the occurrence of a strong additional line between the two centre of mass modes, indicating strong deviations from ideal parabolicity. Also note the broadening and decrease in intensity of the upper cm modes around  $B = 12$  T, indicating the onset of an additional anticrossing.



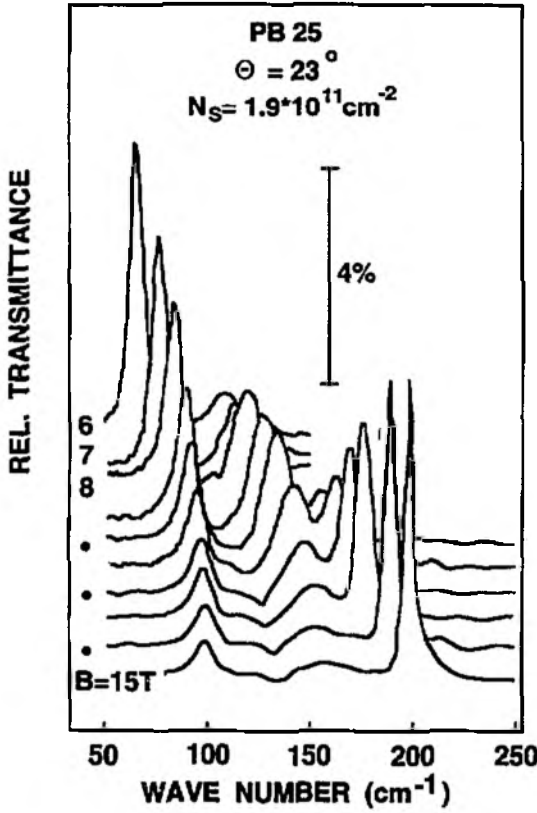


Figure 18. Experimentally obtained spectra for sample PB25 at even lower well filling in tilted magnetic fields  $6 \text{ T} \leq B \leq 15 \text{ T}$ . The anticrossing, as already indicated in figure 17, now has become stronger such that a new line splitting can be clearly resolved.

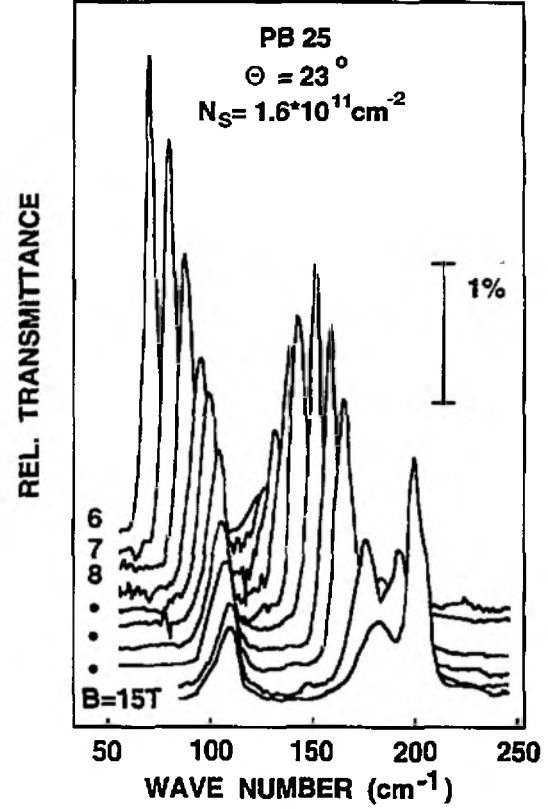


Figure 19. Experimentally obtained spectra for sample PB25 at very low well filling in tilted magnetic fields  $6 \text{ T} \leq B \leq 15 \text{ T}$ . The strong asymmetry of the confining potential (cf figure 12) completely changes the observed spectra with respect to those of figure 16. The simple harmonic oscillator picture is by no means applicable under these experimental conditions.

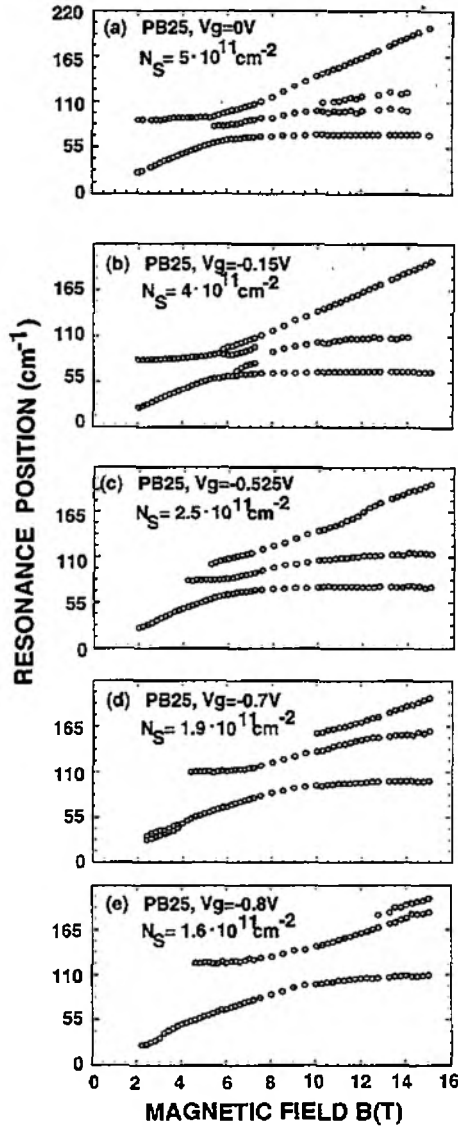
the more those additional lines gain in importance. In figure 17 three distinct lines appear and the onset of a new anticrossing around  $B = 12 \text{ T}$  is observed, being reflected in a strong broadening of the ISR-like line  $\omega_+$  at around  $160 \text{ cm}^{-1}$ . This anticrossing is clearly resolved in the spectra of figures 18 and 19, taken at quite a low carrier density and a strongly deformed potential profile, respectively. Here, the major anti-crossing between the CR- and the ISR-like sloshing modes is shifted upwards in frequency, such that the centre of the gap occurs at considerably higher energies than in the unperturbed case. In figure 20 we summarize all the resonance positions as obtained under different experimental conditions and different well fillings or carrier densities. The harmonic oscillator coupling as derived in equation (10) is still applicable to figure 20(a), of course not considering the additional lines within the gap. This can be regarded as an indication that with decreasing carrier density, or equivalently a more deformed potential profile, the mode character significantly changes and self-consistency as well as the appropriate matrix elements of the problem have to be considered to describe the interaction.

A first approach to explain the extra modes occurring in our experiments has been recently carried out by Dempsey and Halperin [31] using a classical hydrodynamic model to describe the magnetoplasma excitations in a pqw. The electron system confined in the well

in this case is treated as a classical charge fluid with an internal pressure  $p$  proportional to a density  $N - N_c$ , where  $N$  is the density of the electrons and  $N_c$  a density at which the pressure vanishes. Linearizing the dynamical equations and neglecting retardation effects, they calculate the dispersion of the magnetoplasmon frequencies as a function of an in-plane wavevector  $q$ . Applied to our experiment, i.e. for small in-plane  $q$ , they show that at least for the case of a completely filled pqw ( $\eta \approx 1$ ) where finite size effects become important, this model gives an impression of the character of the internal modes of the electron system. Those excitations may be regarded as 'standing-wave'-like bulk magnetoplasmons with an integral number of wavelengths within the electron slab of width  $W_c$ . Thus no longer are only two harmonic oscillators coupled in a tilted field experiment but now one has to take into account the pressure-driven internal oscillations of the electron slab. Such non-local interaction effects are well known for homogeneous 3DES and 2DES. They arise from the inherent finite compressibility of the Fermi gas, the 'Fermi pressure', and lead to corrections for the squared plasma frequency. For an ideal three-dimensional system, the frequencies of these oscillations are then given by

$$\omega_n^2 = \frac{3}{5} v_F^2 n \left( \frac{\pi}{W_c} \right) \quad (13)$$





**Figure 20.** Summary of all the experimentally obtained resonance positions from the tilted field experiment on sample PB25 for different well fillings or gate voltages. With decreasing carrier density the spectra deviate more and more from the prediction of the simple harmonic oscillator picture as represented by equation (10). Additional lines besides the CM modes appear and the whole spectrum is shifted towards higher energies, indicating a 'stiffening' of the confining potential.

where  $v_F$  denotes the Fermi velocity of the electrons of the 'natural' density  $n^+$  in the well. For a strictly two-dimensional system, the prefactor  $3/5$  in equation (13) has to be replaced by  $3/4$  [47]. Such non-local effects become important at small plasmon wavelengths or correspondingly high values of  $q$ . A well known and famous manifestation of it is observed if photons are incident on a boundary of a semi-infinite 3DES. Here it is manifested in a coupling of the incident transverse photons with longitudinal plasmons [48]. Also related to this is the problem of the widely discussed 'additional boundary conditions' (ABC) [49]. A similar non-local interaction has recently also been observed in QDES [2, 6]. For the case of our PQW, the different branches

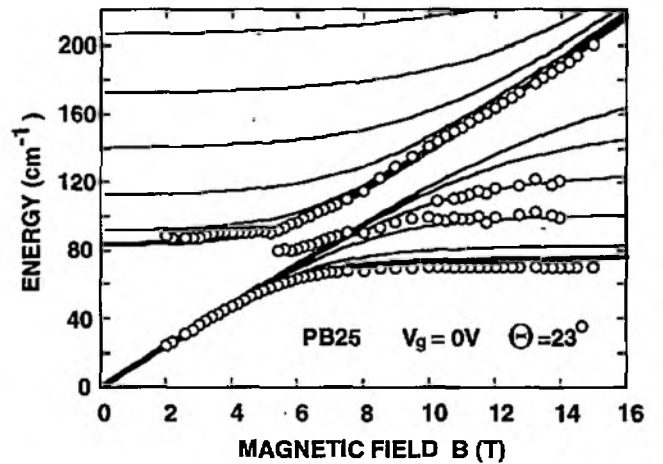
of the coupled system now can be written as

$$\omega_{n\pm} = \left[ \frac{1}{2} \{ (\omega_0^2 + \omega_c^2 + \omega_n^2) \pm [(\omega_0^2 + \omega_c^2 + \omega_n^2)^2 - 4\omega_{c,z}^2(\omega_0^2 + \omega_n^2)]^{1/2} \} \right]^{1/2}. \quad (14)$$

Here,  $\omega_{c,z}$  again denotes the  $z$  component of the cyclotron frequency whereas the other symbols have meanings as defined above. It is important to note that only the modes with  $n = 0$  (CM modes) exhibit a non-zero dipole moment. For symmetry reasons, only these modes should be observable in a FIR transmission experiment. The presence of a gate bias, however, may break this symmetry such that symmetry-forbidden resonances also are detectable in our experiments.

The result of the calculation is shown in figure 21, where we plot the first five internal modes together with the experimental data as extracted from figure 20(a). The thin curves represent the interaction of the Fermi-pressure-driven internal oscillations and the cyclotron resonance, whereas the thick curves are the centre of mass modes as discussed above. The only parameters necessary to make the comparison are  $\omega_0$  and  $W_e$ , which are known independently. Given the simplicity of the model, the agreement between the calculation and the experiment is remarkable. It suggests quite strongly that the actual modes excited in the experiment are closely related to the magnetoplasmon modes as obtained in the simple hydrodynamic approach. In principle, the hydrodynamic calculations should give good results for plasmon-like modes in systems with large, slowly varying electron density, as long as the wavelength of the excitation is large compared with the interparticle spacing [31].

There are, however, some differences between the results of this model and the real experimental data which cannot be explained within this framework. For instance, the model does not predict resonances above the CR-like mode below the point of anticrossing, whereas the



**Figure 21.** Comparison of the theoretical results (curves) obtained employing a classical hydrodynamic approach [31] and our experimental data corresponding to figure 16 (symbols). The additional curves in the calculation are caused by non-local interactions driven by the Fermi pressure and resulting in the occurrence of internal oscillations of the electron slab.

experiment exhibits a quite strong line that slowly levels off with decreasing magnetic field. Furthermore, the agreement between the result of the hydrodynamic model and the experiment becomes worse if the carrier density in the well is considerably reduced as compared with the  $V_g = 0$  V case. Also for different tilt angles, and especially for  $\Theta = 90^\circ$ , the agreement between model and experiment is unsatisfactory [31].

The collective excitations in a PQW can be regarded as representing something in between the true plasmonic collective excitation of a pure 3D system and the intersubband transitions of a pure 2DES, where self-consistent screening leads to an upward shift of the already large transition energies. In a parabolic well the smallness of the self-consistent single-particle energies as compared with the characteristic energy of the bare potential strongly mixes the intersubband transitions, forming collective excitations that occur at much higher energies, and all the plasmon energy arises from the coherent polarization of the electronic system. This strong mixing, together with the self-consistent screening, requires a fully self-consistent calculation of the mode spectrum taking into account not only the centre of mass modes. Such calculations have been recently carried out also by Dempsey and Halperin [33–35] using a self-consistent field approach in local density approximation (LDA-SCF) and, for comparison, also in random phase approximation (RPA). The calculated spectra using both methods, however, only differ by a few per cent in the resonance positions. This indicates that in a PQW exciton-like effects (at least those calculated using a zero-field local exchange potential) are small in comparison with depolarization effects [33, 34]. This is very different from the situation in quasi 2D systems, where depolarization- and exciton-like effects are known to be of the same order of magnitude. Experiments that are sensitive to these contributions, like Raman scattering using polarized and depolarized geometries, certainly promise to be very interesting for a better understanding of the underlying mechanisms.

In their calculations, Dempsey and Halperin chose well parameters to match our real experiments for the sister samples PB25 (hard vertical sidewalls) and PB48 (same curvature but no vertical sidewalls) and find excellent quantitative agreement over a wide range of magnetic field strengths and carrier densities in the wells. Referring the reader to a detailed description of the calculation method in the original articles [33–35], we here restrict ourselves to giving only the essential results.

We start with a description of the spectra of PB25 at a gate bias of  $V_g = 0$  V as shown in figures 16, 20(a) and 21. The most prominent feature as compared with the spectrum of an ‘ideal’ PQW is the occurrence of two extra peaks between the centre of mass modes, which are only little changed with respect to the ‘ideal’ well PB48. A direct comparison of both samples is shown in figure 22, where we plot the measured resonance positions for both samples and identical experimental conditions. Full symbols represent the result for the ‘imperfect’ well PB25 and the open circles those for the ‘ideal’ well PB48.

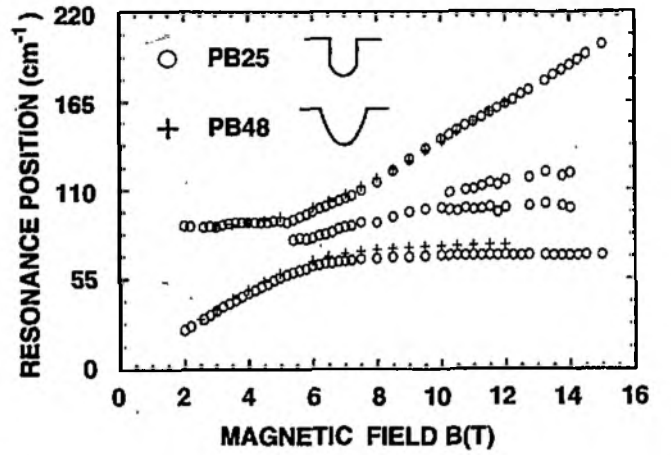
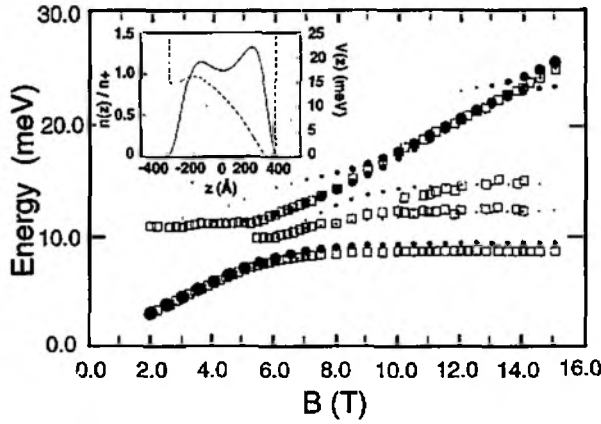


Figure 22. Direct comparison of the extracted resonance positions obtained in a tilted field experiment for two different PQW with the same curvature. In PB25, however, the parabola is truncated by additional vertical sidewalls, leading to the occurrence of additional lines and a slight energetical increase of the low-energy CM mode. The experimental conditions for both samples are the same.

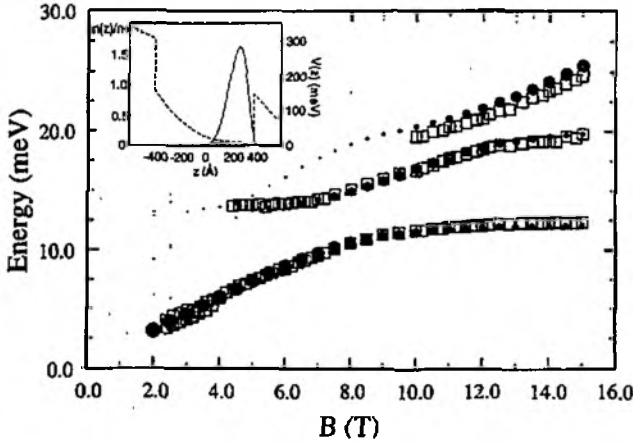
As can be seen, the major differences are the extra peaks and a slight energy decrease of the CM mode  $\omega_-$  for the perturbed sample. The upper CM modes  $\omega_+$  are nearly indistinguishable for both samples.

Dempsey and Halperin accurately reproduced the extra peaks that are observed in the experiment as well as some additional lines and anticrossings by just taking into account the finite size of the well. However, since self-consistent screening strongly mixes the intersubband transitions, it is in general very demanding to associate those peaks in the spectrum with particular transitions. One special case is the upper extra peak in the gap between the CM-like modes. To account for the occurrence of this second extra peak, especially at high magnetic fields, Dempsey and Halperin [34] had to include effects that arise from the finite temperature of the experiment. In a  $T = 0$  calculation this peak, which is associated with the  $1 \rightarrow 4$  intersubband transition, disappears above  $B = 10.5$  T due to a magnetic depopulation of the  $E_1$  subband. Since the single-particle subband separations, however, are so small in a PQW, there is a reasonable occupation of the  $E_1$  subband even at low temperatures. This occupation has a strong effect on the absorption spectrum leading, for example, to the occurrence of the upper extra peak in the spectrum.

The result of Dempsey and Halperin's RPA calculation together with our experimental data is shown in figure 23. The dots are the calculated resonance positions with their size being proportional to the calculated oscillator strength. The boxes are our experimental data. As can be seen, the agreement is close to being perfect as far as the resonance positions are concerned. Also the behaviour of the oscillator strength is calculated quite perfectly as can be seen from figure 16. Given the results of the calculations, the authors also calculated the spectra for a strongly biased PQW, where the electric-field-induced asymmetry becomes the dominant effect on the absorption spectrum. This is shown in figure 24, where again both the



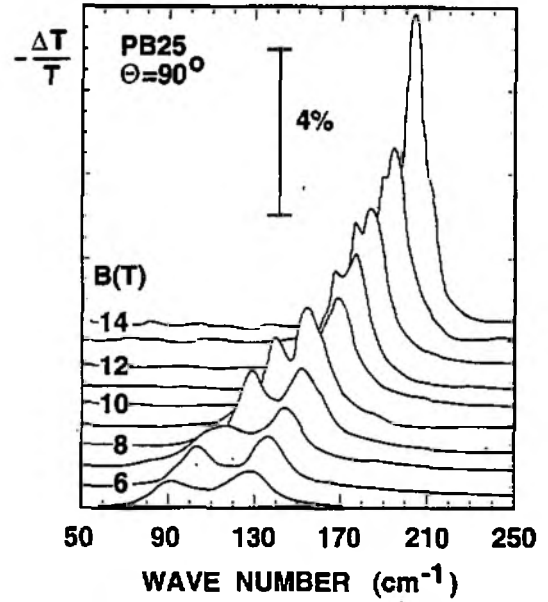
**Figure 23.** Comparison of the result of a fully self-consistent calculation (dots) as described in the text [33, 34] and our experimentally obtained resonance positions (boxes). The area of the dots is proportional to the oscillator strength of the respective lines. The inset depicts the corresponding ground state electron density (full curve, left-hand scale) and self-consistent potential (broken curve, right-hand scale) at  $B = 12$  T. (from [34] with permission.)



**Figure 24.** Comparison between the calculation of [34] (dots) and our experimental results for the partially depopulated well PB25 at a gate bias of  $V_g = -0.7$  V (cf figures 18 and 20(d)). Even for this strongly symmetry-broken case the agreement between the calculation and our experimental result is excellent. The inset depicts the corresponding ground state electron density (full curve, left-hand scale) and the self-consistent potential (broken curve, right-hand scale) at  $B = 12$  T. (From [34] with permission.)

calculated and the experimental resonance positions are shown together for a gate bias of  $V_g = -0.7$  V (cf figure 18), leading to a linear potential gradient of 205 meV across the well. The inset shows the calculated ground-state density and self-consistent potential under these conditions. It is interesting to note that charge accumulation at the edge of the well leads to a maximum electron density that is more than 1.5 times larger than the 'natural' density  $n^+$  given by equation (1).

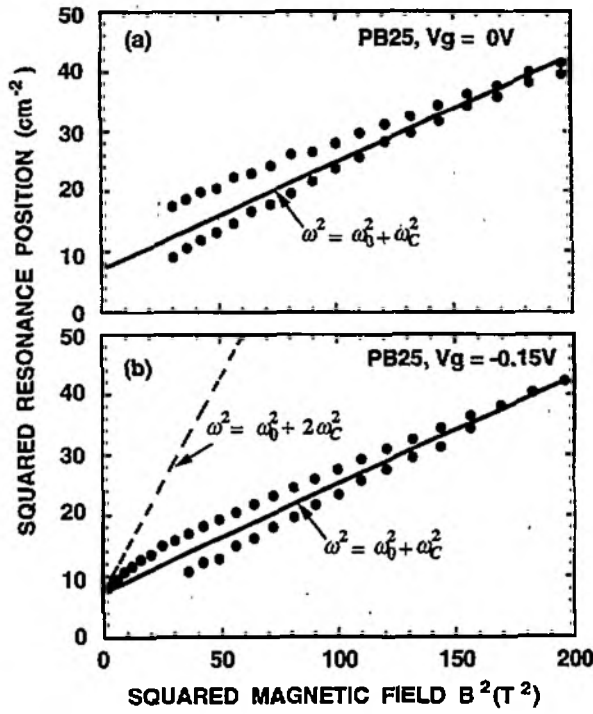
So far we have considered the experiments at tilted magnetic fields where the coupling of the CR to the centre of mass and the internal oscillations of the pqw led to the occurrence of a quite complicated absorption spectrum. For in-plane magnetic fields also, there are



**Figure 25.** Experimental spectra for sample PB25 for  $V_g = 0$  V and  $N_s = 5 \times 10^{11} \text{ cm}^{-2}$  in Voigt geometry (cf figure 9). The magnetic field  $B$  is directed along the plane of the pqw, using normally incident unpolarized FIR. The most striking fact is the occurrence of two lines instead of the single mode of the plasma-shifted CR in an 'ideal' pqw.

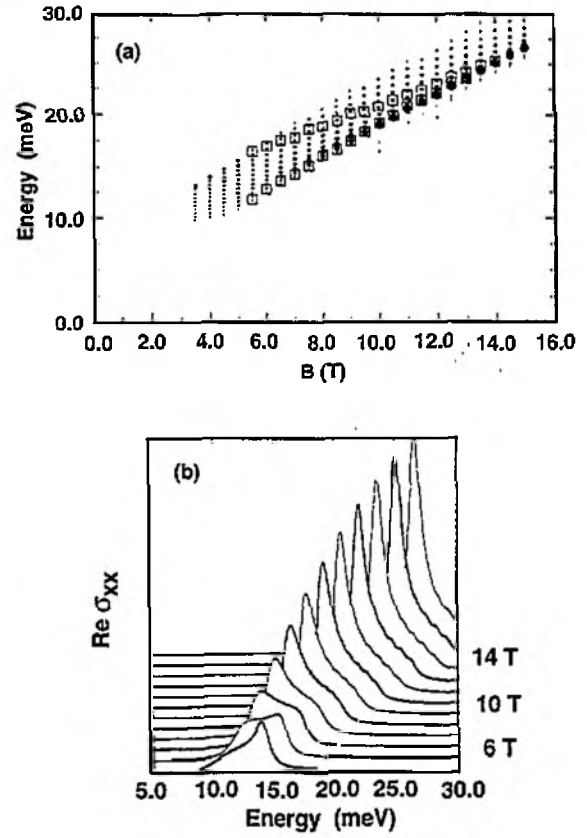
strong deviations from the 'ideal' case. This is a very interesting result, since it can directly be compared with FIR investigations of quantum wires, where the confining potential is not exactly known. An example for the in-plane spectrum of the 'imperfect' pqw PB25 is given in figure 25. The corresponding squared resonance positions versus the squared magnetic field for two different carrier densities in the well are shown in figures 26(a) and (b), respectively. The most striking fact is that now two resonances are observed which are well separated at low magnetic fields and merge at high magnetic fields at the position of the 'unperturbed' hybrid resonance of a pqw in Voigt geometry (see, for example, figure 9). The oscillator strengths of the two resonances vanish for  $B \rightarrow 0$  with the low-energy resonance disappearing earlier. It is interesting to note that, for low magnetic fields, the observed transitions as a function of the magnetic field can be described by  $\tilde{\omega} \approx \sqrt{\omega_0^2 + 2\omega_c^2}$ . A similar behaviour has very recently also been observed in FIR studies of 1D quantum wires [50]. There, the magnetoelectric hybrid mode exhibited a splitting at around  $\Omega \approx \sqrt{2}\omega_c$ , which was attributed to a non-local effect arising from non-parabolic terms in the confining potential. It is interesting to note that this higher-frequency  $\tilde{\omega}$  as well as the apparent mode crossing at  $\Omega \approx \sqrt{2}\omega_c$  corresponds to the situation where  $\omega_0 = \omega_c$ . This is exactly the condition at which the density of states in a pqw in a parallel magnetic field changes from quasi 2D behaviour at low magnetic fields towards quasi 1D behaviour in high magnetic fields [60].

The essential result of Dempsey and Halperin's calculation using a self-consistent-field formalism introduced by Ando [1, 51] is the occurrence of a band of



**Figure 26.** Squared resonance positions for PB25 at two different gate voltages versus the square of the in-plane magnetic field  $B$ . The simple harmonic oscillator picture predicts the full line, representing the plasma-shifted CR as observed in an 'ideal' pqw. Note that in (b) the upper mode intersects the energy axis with a slope approximately given by  $2\omega_c^2$  as described in the text.

transitions instead of the sharp line (cf equation (12)) predicted for an 'ideal' well. The interesting fact is that the oscillator strengths of the single transitions forming a continuum are not distributed symmetrically among these lines. At low magnetic fields, where the electrical quantization is governing the system, the oscillator strength is peaked at the upper edge of the continuum, then moves towards the lower edge until for high magnetic fields both maxima merge. For very large magnetic fields a single line representing the cyclotron resonance is recovered. The point at which the oscillator strength is equal for both lines, again corresponds to a magnetic field, at which  $\Omega \approx \sqrt{2}\omega_c$  or  $\omega_0 = \omega_c$ , respectively. This behaviour is shown in figure 27(a) taken from [35], where the calculated resonance positions and oscillator strengths (dots) together with our experimental data (boxes) at a gate bias of  $V_g = 0$  V are shown. In figure 27(b), the calculated spectrum assuming a phenomenological scattering time  $\tau$  [35] is plotted for comparison. Although the calculated resonance positions match the data of our experiment, we do not really observe the crossover of oscillator strength. Also, there are two well defined resonances in the experimental spectra, whereas the calculation gives a more or less broad continuum with non-symmetrically distributed oscillator strength. This discrepancy between calculation and experiment as well as the physical origin of the interesting anticrossing at  $\omega_0 = \omega_c$  still remains to be solved by future investigations.



**Figure 27.** (a) Comparison of the result of a fully self-consistent calculation (dots) as described in the text [33, 34] and our experimentally obtained resonance positions (boxes) in Voigt geometry. As compared with an 'ideal' system the single line of the plasma-shifted CR is now broadened into a 'continuum' with asymmetrically distributed oscillator strength. The area of the dots is proportional to the oscillator strength of the respective lines. (b) Calculated spectra for the resonances of (a). A phenomenological scattering time has been used to model the absorption lines. (From [35] with permission.)

### 5.3. Finite wavevector experiments

So far we have been considering the response of a parabolically confined electron system to long-wavelength radiation at very small or vanishing wavevector. Now we would like to expand our investigations to the regime of finite  $q$  which is achieved using shorter-period grating couplers. First we present some experimental findings on the complete dispersion of an electron slab of finite width which is comparable to  $q^{-1}$  of the grating coupler. In this context we demonstrate that we are able to excite a whole set of elementary excitations of the system, which are more or less strongly coupled. By the possibility of electrically varying the thickness of the electron slab, and thus in some sense also of changing its dimensionality, we gain access to many fundamental properties of the collective excitation spectrum of an electron system of finite width. As we have discussed in great detail before, the intersubband transitions correspond to charge density oscillations parallel to the direction of confinement and there is a collective mode associated with them, called the intersubband plasmon. For the special case of

an ‘ideal’ pqw, Kohn’s theorem states that this mode is the only one observable in long-wavelength spectroscopy. It represents a ‘sloshing’ of the whole ensemble of electrons like a rigid system and can be represented by the motion of the centre of mass alone.

On the other hand, the collective modes associated with the charge density oscillations perpendicular to the direction of the confinement, i.e. along the ‘free’ direction of the electron slab, are associated with so-called intrasubband plasmons. In a homogeneous infinite plasma these excitations are non-radiative modes in the sense that the spectrum is restricted to the region below the light line, i.e.  $q > \omega/c$  (taking into account retardation also at small  $\omega$  and  $q$ ). Thus no direct coupling with radiation is possible. To couple the plasmon with an electromagnetic wave the latter has to be transformed in a proper way in order to generate a spatially modulated electric field. An effective way to do so is to use grating couplers, which consist of periodic stripes (periodicity  $a$ ) of high- and low-conductivity materials†. Then the incident field, which has a homogeneous  $E_x$  component only, is shortened in the high-conductivity regions of the grating. In the near field of the grating, however, the electromagnetic fields are spatially modulated and consist of a series of Fourier components.

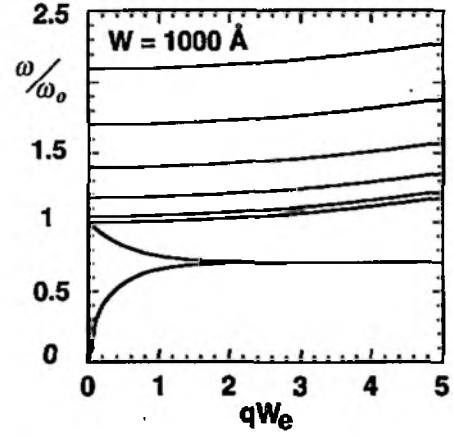
$$e(x, t) = \sum_{n=-\infty}^{\infty} (e_x^n, 0, e_z^n) \exp[i(q_x^n x - \omega t)] \quad (15)$$

with  $q_x^n = n(2\pi/a)$ . Fourier components with this wave-vector can couple to the plasmons if they satisfy their dispersion relation [52]. In a local and strictly two-dimensional treatment, where the wavelength of the excitation is taken to be much larger than the thickness of the electron system, this dispersion of the intrasubband plasmon reads [53]

$$\omega_p^2 = \frac{e^2 N_s q_x^n}{2\bar{\epsilon} m_p}. \quad (16)$$

Here,  $N_s$  again denotes the areal carrier density,  $\bar{\epsilon}$  an effective dielectric function including screening and  $m_p$  a plasmonic effective mass. It is also important that in the near field of the grating  $z$  components  $e_z^n$  of the electric field are induced, which in turn can be used to excite the intersubband-like resonances as discussed in the previous section. The effectiveness of a grating coupler to couple to both modes, however, depends crucially on its design. For instance, the  $n$ th Fourier component of the fields decays with depth like  $\exp(-q_x^n z)$  for  $q_x \gg \omega/c$ . Thus the distance of the grating from the electron system should be small relative to its periodicity, which should be small itself to couple to high-frequency plasmons. Hence, for the special case of a pqw we are somewhat restricted in the choice of the grating coupler, since here, apart from the width of the electron system itself, the wells are usually buried quite deep below the sample.

† In principle, any periodic modulation of the dielectric properties in the vicinity of the electron system, for example a modulation of the system itself, causes a grating coupler effect.

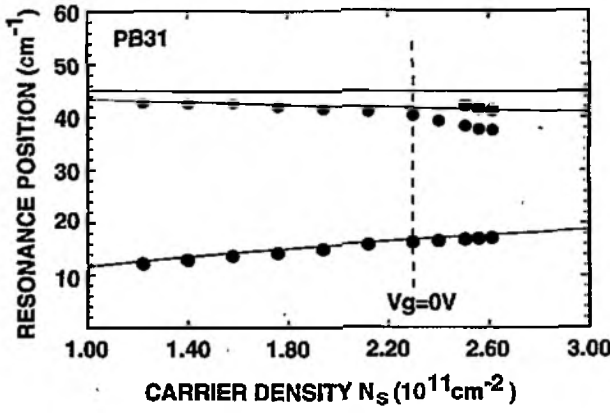


**Figure 28.** Calculated  $B = 0$  uniform-slab dispersion of the collective modes for a pqw as a function of  $qW_e$  using a classical hydrodynamic model [31]. Both bulk-like ( $\omega > \omega_0$ ) and surface-like ( $\omega < \omega_0$ ) excitations can be excited. The surface-like modes degenerate at  $\omega = \omega_0/\sqrt{2}$  for large  $q$ . If the slab width is comparable to  $q^{-1}$ , a strict separation of the mode characters is no longer possible.

Nevertheless, the existence of such surface-plasmon modes on pqw has recently been demonstrated experimentally [36, 37] and their dispersion has been shown to follow equation (16).

The complete excitation spectrum of an electron slab of finite width as realized in pqw has been treated in the hydrodynamic model by Dempsey and Halperin [31]. It is shown in figure 28, where we depict the calculated resonance energies as a function of  $qW_e$ . Here,  $W_e$  again denotes the thickness of the electron slab under consideration. The modes with  $\omega(q) > \omega_0$  represent bulk-like excitations, which can be related to Fermi-driven internal oscillations of the system as already discussed in the previous section. They exhibit a small positive dispersion  $\propto q^2$  as is expected for a 3D bulk plasmon. The two remaining modes with  $\omega(q) < \omega_0$  are surface-like excitations, the lower one being related to the 2D plasmon as described by equation (16) for vanishing thickness. Here it becomes evident that the finite thickness of the electron system certainly has to be included in a theoretical description of the mode character and becomes very important if  $qW_e$  approaches unity [54].

The experiments presented in this section are performed on sample PB31, a 200 nm wide pqw grown as a sister sample to PB26. It has been designed to exhibit a natural resonance frequency of  $\omega_0 \simeq 47 \text{ cm}^{-1}$ . The major difference compared with PB26 is the considerably higher electron mobility of the order of  $3 \times 10^5 \text{ cm}^2 \text{ V}^{-1} \text{ s}^{-1}$ . The carrier density of this sample can be varied between  $N_s = 2.6 \times 10^{11} \text{ cm}^{-2}$  at  $V_g = +0.2 \text{ V}$  and  $N_s = 0$  at  $V_g = -1.3 \text{ V}$ . The experiments presented here were performed using a  $2 \mu\text{m}$  period Ag grating deposited on top of a 6 nm thick semitransparent NiCr gate electrode. Thus, in our experiments  $qW_e < 0.3$  for all gate voltages  $V_g$ , by which the thickness of the layer can be varied according to equation (3). The result of such an experiment is shown in figure 29. Here we plot the extracted resonance positions at  $B = 0$  as a function



**Figure 29.** Experimentally obtained resonance positions of the collective mode spectrum for sample PB31 as a function of the carrier density  $N_s$  or slab width. A  $2\ \mu\text{m}$  periodicity grating coupler has been deposited on top of the sample surface to provide the necessary  $z$  component of the FIR to couple to the intersubband-like mode and also to provide a wavevector  $q$  to couple to the intrasubband plasmon. The lines are the result of the classical hydrodynamic model [31] whereas the full circles represent our experimental data.

of the carrier density  $N_s$  in the sample, which according to equation (3) reflects the thickness of the electron system. The full lines in the figure are the result of the hydrodynamic model for comparison. For low carrier densities only two resonances are observed, representing the surface-like modes at finite wavevector  $q$ . For higher carrier density the first bulk-like plasma mode can also be resolved. The natural frequency  $\omega_0$  of the well has been fitted to  $\omega_0 \simeq 45\ \text{cm}^{-1}$ , which is in good agreement with the one expected from growth. The deviations between the model and the data, especially at high filling of the well, are believed to be related to the uncertainty in the actual width of the electron system, which is simply taken from equation (3). At high well fillings an increase of the carrier density is reflected in an additional charge accumulation near the edges of the well rather than in a further increase of the electronic width. This is also indicated by the fact that the disagreement only occurs at positive bias and by the occurrence of the (symmetry-forbidden) bulk mode. It should be noted that this mode spectrum has been observed in the past also on thin metal films, where the characteristic energies of course are three orders of magnitude higher [55].

We have seen that in a wide PQW the inter- and intrasubband plasma oscillations are energetically of the same order of magnitude. Thus, PQW represent a nearly perfect system to experimentally investigate the mutual interaction between the two types of collective excitations. Resonant interaction of surface plasmons and intersubband resonances was first calculated by Das Sarma [39] employing a random phase approximation frame in a two-band model, and later by Li and Das Sarma [40], and by Gold and Ghazali [41]. Experimentally, it has been observed before by Oelting and co-workers [38] for the case of a 2DES on silicon MOS structures. For a 2DES confined in a triangular potential well, however, the intersubband-resonance energies are usually much larger

than those of intrasubband plasmons for experimentally accessible grating periods and carrier densities such that the coupling is only a second-order effect and leads, for instance, to deviations from equation (16) for large wavevectors  $q$ . By application of uniaxial stress, however, the authors of [38] succeeded in tuning and energetically matching the resonance frequencies. Consequently, they observed resonant interaction between the two excitations and obtained qualitative agreement with the calculation of Das Sarma [39]. From equation (16) we expect the surface-plasmon resonance to occur at  $\hbar\omega_p \approx 19\ \text{cm}^{-1}$  for  $V_g = 0\ \text{V}$  if we use an effective dielectric constant of  $\bar{\epsilon} = 13$  and  $m_p = 0.07\ m_0$ . Since there is a small uncertainty for the actual curvature of a PQW for a given sample, we determine  $\omega_0$  independently for the same sample but before the preparation of the grating, employing tilted field experiments at  $q = 0$ , resulting in  $\hbar\omega_0 \simeq 44 \pm 2\ \text{cm}^{-1}$ . We wish to point out again that for  $q \neq 0$  a strict separation of the modes is no longer possible, since for a finite width of the slab both can have both surface and bulk character. Since we are not able to make both modes degenerate in energy by application of a gate bias alone, we use a perpendicular magnetic field  $B$  to tune the intrasubband plasmon energy. Here, the effect of the cyclotron motion on the surface plasmon leads to the well known classical expression for the magnetoplasmon excitation [56]

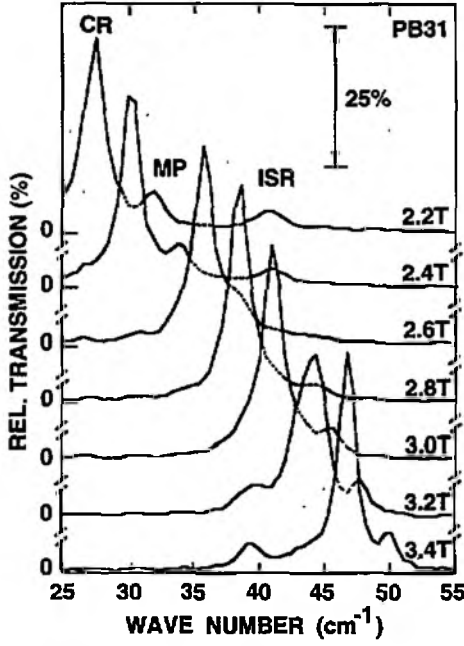
$$\omega_{\text{MP}}^2 = \omega_c^2 + \omega_p^2. \quad (17)$$

The mode character of the surface plasmon, however, is not changed by the magnetic field.

In figure 30 we present a typical set of spectra as obtained experimentally for a gate bias of  $V_g = 0\ \text{V}$ . In this case according to figure 3 at least two electrical subbands are occupied. We depict the relative change in transmission  $-\Delta T/T$  as a function of energy for different magnetic field values  $B$ . For low magnetic fields one observes three absorption lines, which we identify as cyclotron resonance (CR), intrasubband magnetoplasmon (MP) and intersubband-like plasmon (ISR), respectively. With increasing magnetic field both the CR and the MP shift to higher energies according to the above magnetic field dispersion. For  $B \approx 2.8\ \text{T}$ , however, resonant interaction of MP and ISR is observed, as reflected in an anticrossing behaviour.

Figure 31 depicts the extracted resonance positions for all three modes as a function of magnetic field and for three different gate voltages or carrier densities in the well. The full lines are the result of Das Sarma's calculation [39], which we will address below in detail. From the figure it can be seen that the strength of the resonant interaction between the intra- and the intersubband collective modes, represented by an anticrossing gap, obviously depends on the number of carriers or the gate bias. For low carrier density, there is—within the resolution of our experiment—nearly no anticrossing of the two modes observable. Increasing the gate bias, however, opens a gap between the two lines, which becomes larger with increasing carrier density. The intrasubband plasmon frequency  $\omega_p$  (which is identical to  $\omega_{\text{MP}}$  for





**Figure 30.** Typical set of spectra as obtained on a 200 nm wide PQW (PB31) with a 2  $\mu\text{m}$  grating coupler. We plot the relative change in transmission as a function of the FIR energy for different magnetic fields. The spectra have been vertically offset for clarity. At low as well as at high magnetic fields three lines are observed which are interpreted in terms of cyclotron resonance (CR), intrasubband magnetoplasmon (MP) and intersubband plasmon (ISR). Around  $B \approx 2.8$  T the intra- and the intersubband modes interact resonantly, whereas the CR remains unaffected.

$B \rightarrow 0$ ) increases with increasing carrier density  $N_s$ , as expected from equation (16). The parameters  $\omega_{0,p,i}$  given in the inset are the result of a fit to the data, according to the two-band model originally derived for a 2DES by Das Sarma [39]. Using his terms, the interaction of the surface (intrasubband)-plasmon  $\omega_p$  and an intersubband mode  $\omega_{21}$  leads to an expression for the coupled modes

$$\omega_{\pm}^2 = \frac{1}{2} \{ (\omega_{21}^2 + \omega_p^2) \pm [(\omega_{21}^2 - \omega_p^2)^2 + 4\omega_i^4]^{1/2} \}. \quad (18)$$

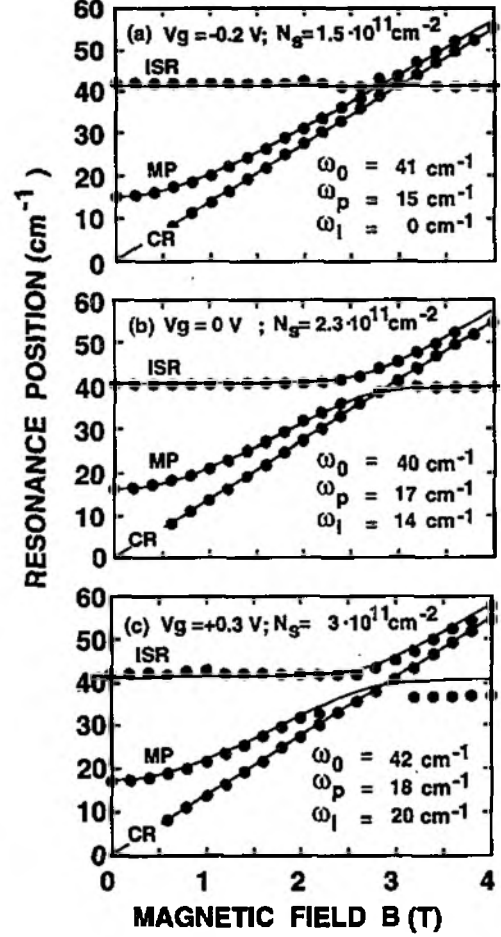
For a two-dimensional space-charge layer  $\hbar\omega_{21} = (E_{21}^2 + W_p^2)^{1/2}$  denotes the depolarization shifted intersubband resonance frequency with

$$W_p = (2N_s E_{21} v_{1212}(q \rightarrow 0))^{1/2}. \quad (19)$$

For a PQW, the description is much simpler since Kohn's theorem states that  $\omega_{21} \equiv \omega_0$ . The frequency

$$\omega_i = \{2N_s^2 E_{21} [v_{1112}(q \rightarrow 0)]^2 / m\}^{1/2} \quad (20)$$

determines the strength of the coupling, where  $E_{21}$  is the self-consistent subband spacing and  $v_{ijkl}$  the matrix elements for Coulomb interaction between the modes  $ij$  and  $kl$  in subbands 1 and 2, respectively. For a symmetric potential well this matrix element turns out to be strictly zero for arbitrary  $q$  if  $i + j + k + l$  is an odd number. Therefore, the two-band model predicts no mode coupling to occur for our PQW. If, however, more than one occupied electrical subband and some asymmetry of the potential are taken into account, this is no longer



**Figure 31.** (a) Experimentally obtained resonance positions of an experiment as shown in figure 30, but for lower carrier density  $N_s$ . In this case presumably only the lowest electrical subband is occupied and the confining potential is symmetric. Within the resolution of our experiment no resonant interaction between the inter- and intrasubband plasmons is observed, which is in agreement with equation (20). (b) Resonance positions as obtained from the spectra of figure 30. The full circles are the experimental results whereas the curves are the result of the calculation involving Das Sarma's two-band model [39] for all three modes. Clearly a resonant coupling of the intra- and intersubband-like modes is observed and results in an anticrossing of the two modes. To obtain best agreement between theory and experiment the parameters as listed in the figure have been used. (c) For comparison: the same result for a more positive gate bias corresponding to a higher electron concentration with at least three occupied subbands. In this case the mode coupling is strongly enhanced as compared with (a) and (b) and the two-band model no longer holds.

true. Employing a more sophisticated three-band model, Li and Das Sarma have shown [40] that in this case the mode coupling indeed recovers due to the interaction of the intrasubband excitation in the different occupied subbands with the respective intersubband modes. Since we are tuning the intrasubband plasmon via the magnetic field as described above,  $\omega_p$  in equation (18) has to be replaced by  $\omega_{MP}$ , and due to the validity of Kohn's theorem  $\omega_{21}$  by  $\omega_0$ , leading to

$$\omega_{\pm}^2 = \frac{1}{2} \{ (\omega_0^2(q) + \omega_{MP}^2(q, N_s, B)) \pm [(\omega_0^2(q) - \omega_{MP}^2(q, N_s, B))^2 + 4\omega_i^4]^{1/2} \}. \quad (21)$$



This result is shown as full curves in figure 31, where we plot it together with the extracted resonance positions for all three modes as a function of the magnetic field  $B$ . Experimentally, special care was taken not to tilt the magnetic field with respect to the normal of the PQW layer since this leads to an additional coupling of the CR and the ISR modes, as has been discussed in the previous sections and which would unnecessarily complicate the study presented here. No such signature is observed in our data. Hence we are sure that the resonant anticrossing between MP and ISR is solely determined by the Coulomb coupling of the two modes. Using the above-mentioned two-band model for simplicity, the coupling is expressed in terms of  $\hbar\omega_i$  as indicated in the insets to obtain optimum agreement with our data. The grating coupler-induced intersubband resonance in this case has, due to its dispersion, a somewhat lower value than the one we extract from  $q = 0$  experiments on the same sample, namely  $\omega_0(q) \approx 41 \text{ cm}^{-1}$ .

In figure 31(a), where the system is in the electrical quantum limit, i.e. when only one subband is occupied, we do not observe a resonant interaction between the two modes at all. Here, the two-band model for a symmetric potential should hold. Moreover, self-consistent calculations show that in this case the confining potential is essentially symmetric. Thus, according to Das Sarma, no coupling is expected. For  $V_g = 0$ , two or even three subbands are occupied but the potential should be still rather symmetric. Here, although not strictly applicable, the data are perfectly reproduced by equation (20), using a coupling constant of  $\omega_i = 14 \text{ cm}^{-1}$ . This value should be compared with a future theoretical calculation for a parabolically confined electron system, which is not available to date.

For even higher well filling up to four subbands are occupied, and the symmetry of the potential is certainly reduced. This could already be deduced from figure 29, where at large positive bias a symmetry-forbidden bulk-like plasmon has been observed. In this case, the resonant interaction is largest, and the simple two-band model is no longer applicable. This is indicated by the bad agreement between the calculation and the experimental data. Up to now we have not been able to recover the predicted mode coupling by breaking the symmetry of the confining potential by application of a very large negative bias. This should occur, since in a non-symmetric potential the matrix element  $v_{1112}$  is not necessarily zero. The main reason is the very small oscillator strength of the resonances at low carrier density, which makes the detection of a mode anticrossing very difficult. In principle this could be overcome by using a PQW with a back-electrode such that the well can be biased without significantly changing the carrier density.

The unique subband spectrum that results if the PQW is subjected to an in-plane magnetic field, namely the hybridization of the cyclotron resonance frequency and the 'natural' frequency  $\omega_0$  arising from the constant curvature of a PQW, leads to the observation of a single well defined frequency ('plasma-shifted CR') given by equation (12). This has been discussed in detail in section 5.1.

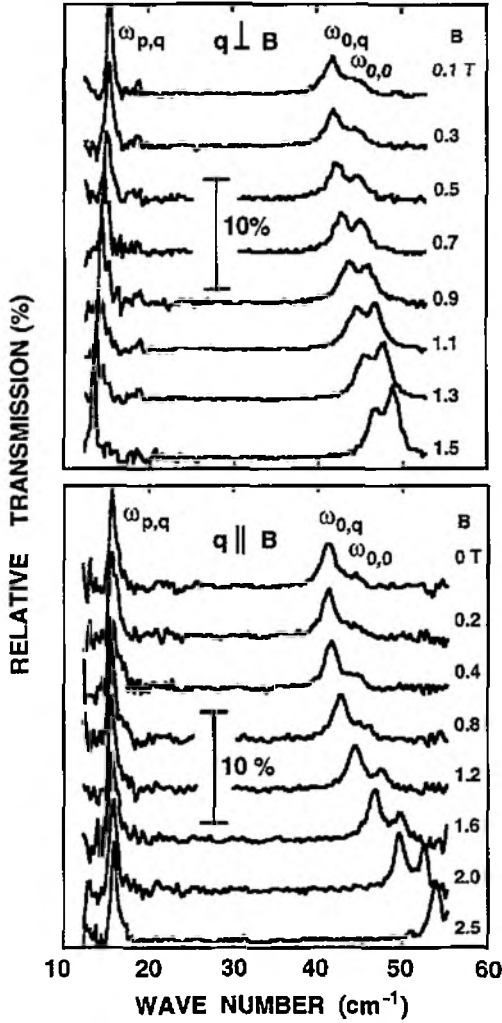
There, we also mentioned the striking similarity of this hybrid mode to the one which is often referred to as 'one-dimensional intersubband resonance' as it is observed in a quantum wire subjected to a perpendicular magnetic field. At finite wavevector, intrasubband-like excitations are also possible, as has been discussed above for the case of a PQW. The same is true for a 1DES as realized by a quantum wire. Here, so-called one-dimensional plasmons can propagate along the free direction of the wire, i.e. normal to the direction of the confinement. Recently, Demel and co-workers [5] succeeded in the observation of such 1D plasmons by investigating the magnetic field dispersion of this mode at finite  $q$ . They produced deep mesa-etched quantum wires with an additional metal grating coupler on top of them. As in a 2DES, the grating coupler allows coupling to internal excitations of the system with the same  $q$ . If subjected to a magnetic field, these modes exhibit a very characteristic negative magnetic field dispersion, indicating the edge-excitation character of this plasmon [57, 58]. The similarity of the band structure of a PQW to a 1DES in parabolic approximation led us to the investigation of such 1D edge plasmons in our samples. As has been shown above, the magnetic-field-induced band structures of both a PQW and a 1DES are quite similar, if the magnetic confinement and the electrical confinement act in the same direction. Thus, our experiments have to be carried out using in-plane fields. At finite  $q$ , as achieved using the grating coupler technique, we expect to observe three different collective modes:

(i) The plasma-shifted cyclotron resonance as discussed in section 5.1, which can be excited by means of the coupling of the CR to the well frequency  $\omega_0$ . This hybrid mode is a  $q = 0$  excitation and shows a characteristic behaviour of the oscillator strength as a function of the magnetic field given by equation (12) (cf figure 9).

(ii) The surface-like excitation at finite  $q$ , which can be regarded as the grating-coupler-excited intersubband plasmon (dimensional resonance) driven by the  $z$  component of the FIR electric field. Since it is directly excited, the oscillator strength of this mode is non-zero at zero magnetic field and, due to its  $q$  dispersion, it has a somewhat lower resonance energy than (i) (cf figures 28, 29).

(iii) The intrasubband surface plasmon which can be related to the 2D plasmon if the thickness of the electron slab is small compared with  $q^{-1}$  (cf equation (16)). This mode is driven by the  $x$  component of the electric field in the proximity of the grating coupler.

Most interesting is the fact that for our sample geometry different orientations of  $q$  with respect to  $B$  are possible. We shall demonstrate that the case  $q \perp B$  is in exact analogy to the one-dimensional plasmon as discussed above. In figure 32 we show a set of typical spectra as obtained for sample PB31 with a  $2 \mu\text{m}$  grating coupler in Voigt geometry. The magnetic field is directed along the free direction of the electron slab, i.e. parallel to the plane of the PQW. In the upper panel we



**Figure 32.** (a) Typical spectra as obtained in transmission and Voigt geometry for different magnetic fields  $B$ . The cases of  $q$  being perpendicular (a) and parallel (b) to  $B$  are depicted. In both experiments we observe three resonances, which are related to the intrasubband plasmon at finite wavevector  $(p, q)$ , the intersubband plasmon at finite wavevector  $(0, q)$ , and the intersubband plasmon at zero wavevector  $(0, 0)$ . The latter is also called plasma-shifted cyclotron resonance. In (a) the resonance  $(p, q)$  has a characteristic negative magnetic field dispersion, whereas  $(0, q)$  and  $(0, 0)$  follow the dispersion for a magnetoelectric hybrid excitation as described in the text. (b) In contrast to (a), for parallel configuration the intrasubband plasmon  $(p, q)$  exhibits no magnetic field dependence as expected from the simple model given by equation (27).

depict the observed spectrum for different magnetic fields with  $q \perp B$ . For low magnetic fields we observe two well defined resonances which we identify as the intrasubband plasmon ( $\omega_{p,q}$ ) and the grating-coupler-induced intersubband-like excitation of the sloshing electron system ( $\omega_{0,q}$ ). With increasing magnetic field this resonance increases in energy, as predicted by equation (12). The lower resonance ( $\omega_{p,q}$ ), however, exhibits a negative  $B$ -field dispersion, i.e. with increasing  $B$  the resonance position shifts to lower energies. For higher magnetic fields a second mode ( $\omega_{0,0}$ ) develops at a slightly higher energy than the grating-coupler-

induced ISR ( $\omega_{0,q}$ ). We identify this line with the CR-ISR hybrid at  $q = 0$ . This is also indicated by the typical behaviour of the oscillator strength of this mode following equation (12).

In the lower panel of figure 32 the result of the corresponding experiment with  $q \parallel B$  is shown for comparison. Qualitatively, no differences from  $q \perp B$  are observed for either ISR-like mode. The intrasubband plasmon, however, does not shift in energy at all with increasing magnetic field. This is the direct consequence of the magnetic-field-induced anisotropic band structure occurring under these experimental conditions. Omitting the spin, the initial eigenenergy equation for a PQW subjected to an in-plane magnetic field reads [59]

$$\left( \frac{1}{2m^*} (p + eA)^2 + \frac{m^* \omega_{0,0}^2}{2} z^2 \right) \Psi = E \Psi \quad (22)$$

where  $m^* \omega_{0,0}^2/2$  characterizes the parabolic potential in the growth ( $z$ ) direction and  $\omega_{0,0}$  is the natural frequency of the parabolic well. At finite wavevector  $q$ , the mode exhibits a dispersion [31] which is determined by the quantity  $qW_e$ ,  $W_e$  again being the width of the electron system in the direction of confinement

$$\omega_{0,q}^2 = \frac{\omega_{0,0}^2}{2} [1 + \exp(-2qW_e)]. \quad (23)$$

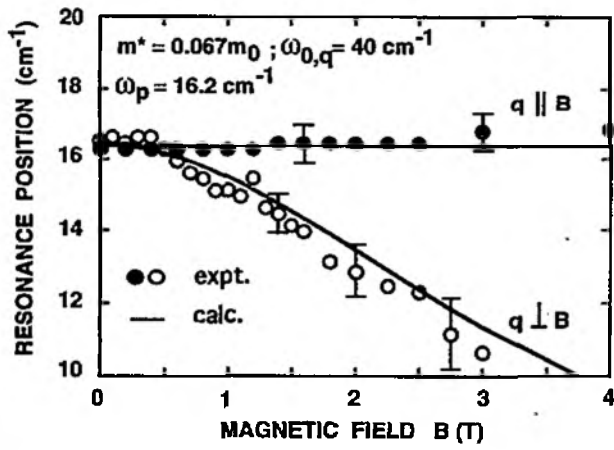
Taking  $A = -(Bz, 0, 0)$ , and separating the variables in the usual way, one obtains from equation (21)

$$\left( \frac{-\hbar^2}{2m^*} \frac{d^2}{dz^2} + \frac{m\Omega^2}{2} \bar{z}^2 \right) f(\bar{z}) = \bar{E}(\bar{z}) \quad (24)$$

where  $\Omega^2 = \omega_{0,q}^2 + \omega_c^2$  is the effective hybrid frequency at finite  $q$ , and  $\bar{z} = z - z_0$  with  $z_0 = \hbar k_x \omega_c / m^* \Omega^2$ . The resulting energy dispersion then turns out to be given by

$$E = \hbar \Omega (n + \frac{1}{2}) + \frac{\hbar^2 k_x^2}{2m^*} \frac{\omega_{0,q}^2}{\Omega^2} + \frac{\hbar^2 k_y^2}{2m^*}. \quad (25)$$

This dispersion describes a harmonic oscillator-like spectrum in the confining direction of the parabolic potential with a characteristic frequency  $\Omega$ , representing the intersubband-type collective excitation that has been discussed in detail before. The free motion in the plane of the QDES is represented by the quasimomenta  $k_x$  and  $k_y$ . Equation (25) has exactly the same form for a 1DES (quantum wire) in parabolic approximation if one replaces the term containing  $k_y$  by the 2D subband energy of the 'starting material' 2DES. The term containing  $k_x$  is then related to so-called one-dimensional plasmons propagating along the wire [5]. The interesting fact for a PQW, however, is the occurrence of an anisotropic band structure in the plane of the electron system with respect to the direction of the magnetic field. The same anisotropy has been observed before, although as a much weaker effect, for high-quality 2DES on GaAs/AlGaAs heterostructures [60]. The theoretical description in that case, however, is rather complex and not straightforward [61]. Using equations (25) one can define a very simple expression for the effective plasmon mass for a PQW and



**Figure 33.** Resonance positions as extracted from figure 32 for both orientations of the intrasubband plasmon wavevector  $q$  with respect to  $B$ . They reflect the magnetic-field-induced anisotropy of the plasmon mass. Symbols represent the experimental data, whereas the full curves are the result of the simple model as described in the text. The parameters used, which are in good agreement with the ones expected, are given in the figure.

the geometry under consideration

$$m_{\perp} = m^* \left( 1 + \frac{\omega_c^2}{\omega_{0,q}^2} \right) \text{ and } m_{\parallel} = m^* \quad (26)$$

in the plane of the electron system. The subscript symbols for  $m$  indicate the direction with respect to the magnetic field. With increasing magnetic field the 'perpendicular' effective mass renormalizes and increases quadratically. The effective mass parallel to the magnetic field remains unaltered and is given by  $m^*$ . Using this expression for the plasmon mass we obtain the magnetic field dispersion of the surface plasmon

$$\omega_{p,q}^2(q_{\perp}) = \omega_p^2 \left( 1 + \frac{\omega_c^2}{\omega_{0,q}^2} \right)^{-1} \quad \omega_{p,q}^2(q_{\parallel}) = \omega_p^2. \quad (27)$$

The result is shown in figure 33, where we plot the extracted resonance positions of  $\omega_{p,q}$  for both principal orientations of  $q$  and  $B$  as a function of the magnetic field. For high magnetic fields ( $B > 3$  T) we are not able to follow the negative dispersion of  $\omega_{p,q\perp}$  since we are approaching the noise limit of our spectrometer close to  $10 \text{ cm}^{-1}$ . The magnetic-field-independent resonance  $\omega_{p,q}$  for  $q \parallel B$ , however, does not deviate significantly from its low-field behaviour up to  $B = 15$  T. These data have been omitted in the plot for clarity. Note that no fit parameter has been used since all quantities can be measured independently.

## 6. Summary

In the present article, we give a comprehensive review of our recent experimental investigations on the far-infrared response of an electron system which is confined in an external harmonic potential. Such structures have been realized in so-called parabolic quantum wells which can be fabricated using modern molecular beam growth

techniques. The characteristics of such electron systems are of great interest since most of the currently available so-called nanostructures can be described in good approximation in a parabolic model. Also, the theoretical description of the properties of parabolically confined electron systems is mostly straightforward due to the unique properties of the quantum mechanical harmonic oscillator. Many fundamental properties of it were investigated theoretically in the early days of quantum mechanics, for example the effect of a magnetic field on its spectrum [62].

Here we have mainly focused on the collective excitation spectra of parabolically confined electron systems employing long-wavelength spectroscopy. First, we concentrated on the spectrum of what we call 'ideal PQW', where the confining potential is very close to being real harmonic. We then discussed the generalized Kohn theorem, which was formulated in connection with experiments on PQW and subsequently had been successfully applied also to the description of the spectral behaviour of quantum wires and dots. A somewhat frustrating result, however, was that the spectral response of parabolically confined systems does not depend on electron-electron interactions. This makes it impossible to uncover fine structure in geometries like 'quantum dot atoms' if the confining potential is harmonic. The study of PQWs, where we intentionally induced some degree of non-parabolicity, however, clarified the situation a lot: once we know about the spectrum of an ideal well, we can directly compare it with the more complex spectrum of an 'imperfect' PQW and gain some insight into the fine structure of the collective modes. Due to the relative simplicity of the confining potentials, the theoretical description is relatively straightforward. Our experimental results have been compared with those obtained in a classical hydrodynamic model as well as with those obtained in more sophisticated approaches and excellent agreement has been obtained. These studies may also be very useful in the understanding of the collective spectrum of quantum wires and dots, where the confining potential is not known *a priori*.

The study of the collective excitation spectrum of an electron slab also included investigations at finite wavevector and scrutiny of the mode dispersion. For an electron system of finite width, a whole set of collective excitations which are strongly coupled becomes accessible. In first-order approximation the excitations can be divided into surface- and bulk-like modes, each of which exhibits a characteristic dispersion. We studied the mutual interaction of inter- and intrasubband collective modes, which is not possible in this simplicity for a 2DES. Here, too, we could directly compare our results with those predicted and in part already experimentally observed on quantum wires and dots. The same is true for the characteristic magnetic field dispersion of intrasubband plasmons if the PQW is subjected to an in-plane magnetic field. We gain direct access to the magnetic-field-induced anisotropy of the band structure which is reflected in a renormalization of the effective mass. The case where the effective plasmon mass is

renormalized due to the strong interplay between magnetic and electrical confinement could directly be related to the recent observation of one-dimensional plasmons propagating along quantum wires.

The striking similarity of many properties of the electron system confined in a pqw to those in quantum wires and dots certainly makes our studies a valuable tool with which to understand and investigate many other interesting features that cannot so easily be accessed in those nanostructures and provides valuable information for the future direction this rapidly developing field of research.

## Acknowledgments

It is a great pleasure for us to gratefully acknowledge many and very fruitful discussions and disputes during the course of this work with E Batke, K Campman, S Das Sarma, J Dempsey, E G Gwinn, R Haupt, P F Hopkins, B I Halperin, K Karaii, W Kohn, H Kroemer, U Merkt, Ch Peters, M Shayegan, L Wendler and R M Westervelt. We would also like to specially acknowledge the encouraging and enthusiastic influence of J P Kotthaus during many enlightening discussions. AW and KE thank the Center for Quantized Electronic Structures (QUEST) at the University of California, Santa Barbara for hospitality during a sabbatical stay. This work has been sponsored in part by the Deutsche Forschungsgemeinschaft, the Volkswagen Stiftung, and in part by the US Air Force Office of Scientific Research under contract no AFOSR-88-099.

## References

- [1] For an excellent review on the electronic properties of low-dimensional systems, see, for example, Ando T, Fowler A B and Stern F 1982 *Rev. Mod. Phys.* **54** 437
- [2] See, for example, Heitmann D 1986 *Two-Dimensional Systems: Physics and New Devices* ed G Bauer et al (Berlin: Springer) p 285
- [3] For a recent review see, for example, Hansen W, Merkt U and Kotthaus J P 1992 *Semiconductors and Semimetals* vol 35 ed R K Willardson et al (San Diego: Academic) p 279
- [4] Hansen W, Horst M, Kotthaus J P, Merkt U, Sikorski Ch and Ploog K 1987 *Phys. Rev. Lett.* **58** 2586
- [5] Demel T, Heitmann D, Grambow P and Ploog K 1990 *Phys. Rev. Lett.* **64** 788
- [6] Sikorski Ch and Merkt U 1989 *Phys. Rev. Lett.* **62** 2164
- [7] Due to the varying Al content in a pqw the wavefunctions of different subbands extend into regions of a different average effective mass, which influences the position of the cyclotron resonance. See, for example:  
Wixforth A, Sundaram M, Donnelly D, English J H and Gossard A C 1990 *Surf. Sci.* **228** 489  
Karrai K, Ying X, Drew H D and Shayegan M 1990 *Phys. Rev. B* **42** 9732
- [8] Wixforth A, Sundaram M, English J H and Gossard A C 1990 *Proc. 20th Int. Conf. on the Physics of Semiconductors* vol II, ed E M Anastassakis and J D Joannopoulos (Singapore: World Scientific) p 1705
- [9] Wixforth A, Sundaram M, Ensslin K, English J H and Gossard A C 1991 *Phys. Rev. B* **43** 10000
- [10] Wixforth A, Sundaram M, Ensslin K, English J H and Gossard A C 1992 *Surf. Sci.* **267** 523
- [11] Kaloudis M, Ensslin K, Wixforth A, Sundaram M, English J H and Gossard A C 1992 *Phys. Rev. B* **46** 12469
- [12] Wixforth A, Kaloudis M, Sundaram M and Gossard A C 1992 *Solid State Commun.* **84** 861
- [13] Sundaram M, Gossard A C, English J H and Westervelt R M 1988 *Superlatt. Microstruct.* **4** 683; see also  
Shayegan M, Sajoto T, Santos M and Silvestre C 1988 *Appl. Phys. Lett.* **53** 791
- [14] Halperin B I 1987 *Japan. J. Appl. Phys.* **26** 1913
- [15] Celli V and Mermin N D 1965 *Phys. Rev.* **140** A839
- [16] Karrai K, Drew H D, Lee H W and Shayegan M 1989 *Phys. Rev. B* **39** 1426
- [17] Karrai K, Ying X, Drew H D and Shayegan M 1989 *Phys. Rev. B* **40** 12020
- [18] Kohn W 1961 *Phys. Rev. B* **123** 1242
- [19] Brey L, Johnson N F and Halperin B I 1989 *Phys. Rev. B* **40** 647
- [20] Yip S K 1991 *Phys. Rev. B* **43** 1707
- [21] Miller R C, Gossard A C, Kleinmann D A and Muntaneau O 1984 *Phys. Rev. B* **29** 3740
- [22] Sundaram M, Chalmers S A, Hopkins P F and Gossard A C 1991 *Science* **254** 1326
- [23] Eisenstein J P 1992 *Superlatt. Microstruct.* **12** 107
- [24] Sundaram M, Wixforth A, Geels R S, Gossard A C and English J H 1991 *J. Vac. Sci. Technol. B* **9** 1524
- [25] See, for example, Wixforth A, Sundaram M, Ensslin K, English J H and Gossard A C 1990 *Appl. Phys. Lett.* **56** 454
- [26] Gwinn E G, Westervelt R M, Hopkins P F, Rimberg A J, Sundaram M and Gossard A C 1989 *Phys. Rev. B* **39** 6260
- [27] Ensslin K, Wixforth A, Sundaram M, Hopkins P F, English J H and Gossard A C 1993 *Phys. Rev. B* **47** 1366
- [28] Karrai K, Ying X, Drew H D, Santos M, Shayegan M, Yang S R E and MacDonald A H 1991 *Phys. Rev. Lett.* **67** 3428
- [29] Schlesinger Z, Hwang J C M and Allen S J Jr 1983 *Phys. Rev. Lett.* **50** 2098; see also  
Wieck A D, Maan J C, Merkt U, Kotthaus J P, Ploog K and Weimann G 1987 *Phys. Rev. B* **35** 4145
- [30] Sundaram M, Wixforth A, Hopkins P F and Gossard A C 1992 *J. Appl. Phys.* **72** 1460
- [31] Dempsey J and Halperin B I 1992 *Phys. Rev. B* **45** 1719
- [32] Brey L, Dempsey J, Johnson N F and Halperin B I 1990 *Phys. Rev. B* **42** 1240
- [33] Dempsey J and Halperin B I 1992 *Phys. Rev. B* **45** 3902
- [34] Dempsey J and Halperin B I 1993 *Phys. Rev. B* **47** 4662
- [35] Dempsey J and Halperin B I 1993 *Phys. Rev. B* **47** 4674
- [36] Asmar N G and Gwinn E G 1992 *Phys. Rev. B* **46** 4752
- [37] Pinsukanjana P R, Gwinn E G, Dobson F, Yuh E L, Asmar N G, Sundaram M and Gossard A C 1992 *Phys. Rev. B* **46** 7284
- [38] Oelting S, Heitmann D and Kotthaus J P 1986 *Phys. Rev. Lett.* **56** 1846
- [39] Das Sarma S 1984 *Phys. Rev. B* **29** 2334
- [40] Li Q and Das Sarma S 1989 *Phys. Rev. B* **40** 5680
- [41] Gold A and Ghazali A 1990 *Phys. Rev. B* **41** 8318
- [42] Batke E and Heitmann D 1984 *Infrared Phys.* **24** 189
- [43] Mann J C 1984 *Two Dimensional Systems: Heterostructures and Superlattices* ed G Bauer et al (Berlin: Springer) p 183
- [44] Merlin R 1987 *Solid State Commun.* **84** 99

- [45] Gwinn E G, Hopkins P F, Rimberg A J, Westervelt R M, Sundaram M and Gossard A C 1990 *Phys. Rev. B* **41** 10 700
- [46] Laux S E, Frank D J and Stern F 1988 *Surf. Sci.* **196** 101
- [47] Stern F 1967 *Phys. Rev. Lett.* **18** 546
- [48] Anderegg M, Feuerbach B and Filton B 1971 *Phys. Rev. Lett.* **27** 1565
- [49] Sauter F 1967 *Z. Phys.* **203** 488  
Melnih A R and Harrison M J 1967 *Phys. Rev. Lett.* **21** 85
- [50] Drexler H, Hansen W, Kottaus J P, Holland M and Beaumont S P 1992 *Phys. Rev. B* **46** 12 849
- [51] Ando T 1975 *J. Phys. Soc. Japan* **39** 411; 1978 *J. Phys. Soc. Japan* **44** 475
- [52] Heitmann D 1987 *Physics and Applications of Quantum Wells and Superlattices (NATO ASI Ser. B: Physics 170)* ed E E Mendez and K von Klitzing (New York: Plenum) pp 317–46
- [53] Stern F 1967 *Phys. Rev. Lett.* **18** 546; for a general review see also  
Chaplik A V 1985 *Surf. Sci. Rep.* **5** 289
- [54] Batke E, Heitmann D and Tu C W 1986 *Phys. Rev. B* **34** 6951
- [55] For a review see, for example, H Raether 1988 *Surface Plasmons* (Berlin: Springer)
- [56] Chaplik A V 1972 *Sov. Phys.-JETP* **35** 395
- [57] Eliasson G, Wu J W, Hawrylak P and Quinn J J 1986 *Solid State Commun.* **60** 41
- [58] Mast D B, Dahm A J and Fetter A L 1985 *Phys. Rev. Lett.* **54** 1706
- [59] Zawadzki W 1989 *High Magnetic Fields in Semiconductor Physics II* ed G Landwehr (Berlin: Springer) p 220
- [60] Batke E and Tu C W 1986 *Phys. Rev. B* **34** 3027
- [61] Stern F 1968 *Phys. Rev. Lett.* **21** 1687
- [62] Fock V 1928 *Z. Phys.* **47** 446